ESC European Society of Cardiology

Cardiovascular Research (2022) **00**, 1–14
https://doi.org/10.1093/cvr/cvac108

# Nogo-A reduces ceramide *de novo* biosynthesis to protect from heart failure

**Linda Sasset [1†], Onorina Laura Manzo[1,2†], Yi Zhang [1,3†], Alice Marino [1], Luisa Rubinelli[1], Maria Antonietta Riemma[1,2], Madhavi Latha S. Chalasani [4], Dragos C. Dasoveanu [4], Fiorentina Roviezzo[2], Stanislovas S. Jankauskas [5], Gaetano Santulli [5], Maria Rosaria Bucci[2], Theresa T. Lu[4], and Annarita Di Lorenzo [1*]**

[1]Department of Pathology and Laboratory Medicine, Cardiovascular Research Institute, Brain and Mind Research Institute, Weill Cornell Medicine, 1300 York Avenue, New York, NY 10065, USA; [2]Department of Pharmacy, School of Medicine, University of Naples Federico II, via Domenico Montesano 49, Naples 80131, Italy; [3]Department of Physiology and Pathophysiology, School of Basic Medical Sciences, Xi'an Jiaotong University Health Science Center, Xi'an, Shaanxi 710061, China; [4]Department of Microbiology and Immunology, Autoimmunity and Inflammation Program, Hospital for Special Surgery Research Institute, Weill Cornell Medicine, New York, NY 10065, USA; and [5]Department of Medicine (Cardiology) and Department of Molecular Pharmacology, Wilf Family Cardiovascular Research Institute, Einstein Institute for Aging Research, Fleischer Institute for Diabetes and Metabolism (FIDAM), Einstein-Mount Sinai Diabetes Research Center (ES-DRC), Albert Einstein College of Medicine, New York, NY 10461, USA

*Received 21 February 2021; revised 24 May 2022; accepted 14 June 2022; online publish-ahead-of-print 11 July 2022*

**Time of primary reviews: 36 days**

**Aims** Growing evidence correlate the accrual of the sphingolipid ceramide in plasma and cardiac tissue with heart failure (HF). Regulation of sphingolipid metabolism in the heart and the pathological impact of its derangement remain poorly understood. Recently, we discovered that Nogo-B, a membrane protein of endoplasmic reticulum, abundant in the vascular wall, down-regulates the sphingolipid *de novo* biosynthesis via serine palmitoyltransferase (SPT), first and rate liming enzyme, to impact vascular functions and blood pressure. Nogo-A, a splice isoform of Nogo, is transiently expressed in cardiomyocyte (CM) following pressure overload. Cardiac Nogo is up-regulated in dilated and ischaemic cardiomyopathies in animals and humans. However, its biological function in the heart remains unknown.

**Methods and results** We discovered that Nogo-A is a negative regulator of SPT activity and refrains ceramide *de novo* biosynthesis in CM exposed to haemodynamic stress, hence limiting ceramide accrual. At 7 days following transverse aortic constriction (TAC), SPT activity was significantly up-regulated in CM lacking Nogo-A and correlated with ceramide accrual, particularly very long-chain ceramides, which are the most abundant in CM, resulting in the suppression of 'beneficial' autophagy. At 3 months post-TAC, mice lacking Nogo-A in CM showed worse pathological cardiac hypertrophy and dysfunction, with ca. 50% mortality rate.

**Conclusion** Mechanistically, Nogo-A refrains ceramides from accrual, therefore preserves the 'beneficial' autophagy, mitochondrial function, and metabolic gene expression, limiting the progression to HF under sustained stress.



* Corresponding author. Tel: +1 212 746 6476; fax: +1 212 746 2290, E-mail: and2039@med.cornell.edu
† These authors contributed equally to the study.

## Graphical Abstract

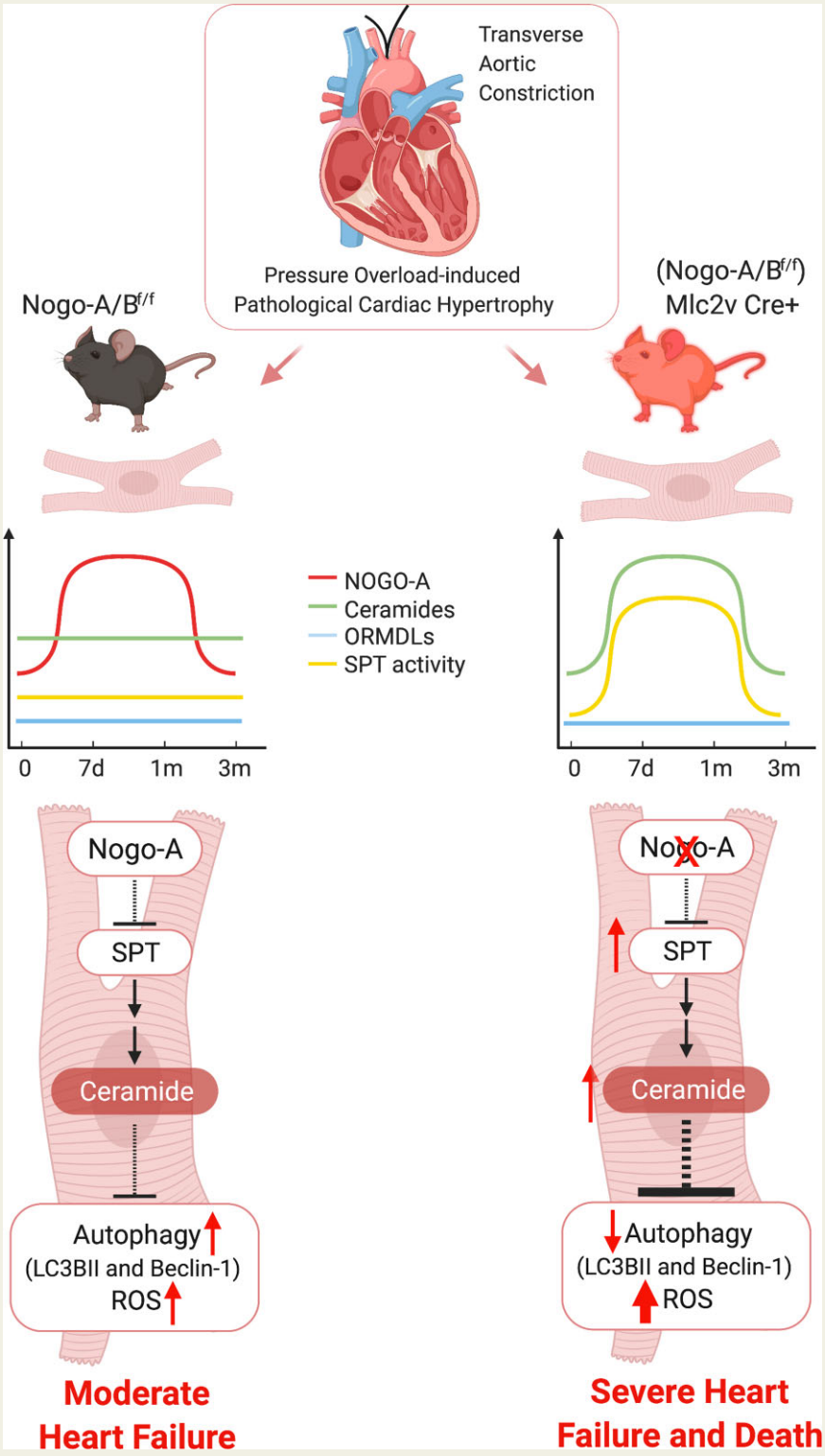


**Keywords** Heart failure • Sphingolipid metabolism • Ceramide • Autophagy • Mitochondrial function

# 1. Introduction

Despite the progress in therapies and preventions, heart failure (HF) still affects about 26 million people worldwide, with even more alarming projections.[1] Altered sphingolipid (SL) metabolism has been implicated in the pathogenesis of HF.[2–4] SL are both building blocks of eukaryotic cell membranes and potent signalling molecules.[5] The SL ceramides regulate multiple cellular processes, including apoptosis and autophagy.[6,7] Plasma ceramides are elevated in hypertension,[8] HF,[9–11] and Type 2 diabetes,[12,13] and have been identified as predictor of major cardiovascular events in patients with and without coronary artery diseases.[14–16]

Growing evidence indicates a critical role of ceramides in cardiac lipotoxicity and HF.[17] Myocardial ceramide levels are increased in models of lipotoxic cardiomyopathy[2,18–20] and ischaemic cardiomyopathy,[11,21] in animals and humans. Russo *et al.*[22] reported that the increase of myocardial C14:0-ceramide, the least abundant in the heart, contributed to lipotoxic cardiomyopathy in mice, in part by increasing autophagy and cell death. In the myocardium of patients affected by HF total ceramides, but not C14:0-ceramide, were significantly elevated compared with control subjects.[11] Although further studies are needed to underpin ceramide-specific functions in cardiomyocyte (CM) biology, there is a general consensus on the contribution of ceramide to lipotoxic-mediated cardiomyophaty.[23] On the contrary, the role of ceramides in pathological cardiac hypertrophy in response to haemodynamic stress is virtually unknown.

Autophagy is regarded as a protective mechanism of the heart, preserving its structure and functions.[24–26] Haemodynamic stress activates autophagy to function as 'damage control' mechanism of the heart. However, in the failing heart autophagy is suppressed contributing to HF.[25,27] To date, how ceramide metabolism is regulated in the heart under haemodynamic stress and its contribution to cardiac damage remain poorly understood.

In ischaemic conditions, Ji *et al.*[11] demonstrated that the *de novo* biosynthesis is mainly accountable for cardiac ceramide elevation, suggesting the inhibition of the *de novo* pathway as a potential therapeutic strategy. A study from Lee and colleagues demonstrated that the loss of serine palmitoyltransferase (SPT) subunit 2 (*Sptlc2*) specifically in CM, impairing the *de novo* production, led to dilated cardiomyopathy,[28] suggesting that ceramide production is necessary for cardiac health. These findings underline the importance of ceramide homeostasis in preserving heart functions.

Thus, understanding how cardiac SL homeostasis is maintained, and the pathological consequences of its derangement, are of fundamental importance to develop therapeutic strategies aiming to restore 'homeostasis' and limit the progression to HF.

In this regard, our laboratory discovered that Nogo-B, a membrane protein of the endoplasmic reticulum, binds to and inhibits SPT, the first and rate-limiting enzyme of *de novo* SL biosynthesis.[29,30] Nogo-B is highly expressed in blood vessels[29] and mice lacking endothelial Nogo-B are protected from hypertension,[29] inflammation,[31] and pathological cardiac hypertrophy.[32]

Nogo-A is the splice isoform of Nogo and mainly expressed in the central nervous system.[33] We showed that under haemodynamic stress, CM express Nogo-A already at 3 days post-transverse aortic constriction (TAC).[32] Multiple other studies reported an up-regulation of *Rtn4* gene (also known as Nogo) in dilated and ischaemic cardiomyopathies, in animals and humans.[34–39] *Rtn4* expression is increased in five different models of cardiomyopathy including pressure overload.[38] Hence, Nogo has been regarded as potential biomarker of HF. To date, the biological role of Nogo-A in the heart remains virtually unknown.

This study investigates whether Nogo-A protects the heart from failure, and underlying mechanisms. We found that mice lacking Nogo-A specifically in CM manifested a severe dilated cardiomyopathy and heart dysfunction during pressure overload, with mortality rate of ~50% vs. control mice. Mechanistically, in pressure overloaded hearts the loss of Nogo-A-mediated inhibition on SPT leads to ceramide accrual in CM, which suppresses the onset of 'protective autophagy', impairs mitochondrial functions and compensatory expression of metabolic genes, contributing to severe HF.

# 2. Methods

## 2.1 Animals

Nogo-A/B floxed mice (Nogo-A/B$^{f/f}$) were generated as previously described.[29] A mouse strain lacking Nogo-A/B specifically in CMs was generated by crossing Nogo-A/B$^{f/f}$ mice with transgenic mice in which the expression of Cre recombinase was under the promoter of ventricular-specific isoform myosin light chain 2 (Mlc2v-Cre),[40,41] hereafter referred to as (Nogo-A/B$^{f/f}$)Mlc2v-Cre+. Mlc2v-Cre mice were kindly provided by Dr Frank Giordano, Yale School of Medicine. Nogo-A/B-deficient mice have been previously described.[42] For all the experiments, age- and gender-matched littermates were used. All protocols and experimental procedures were performed in accordance with the NIH guidelines for the care and use of laboratory animals and approved by the Institutional Animal Care and Use Committee of Weill Cornell Medicine. For tissue collection, mice were euthanized by excess carbon dioxide administration.

## 2.2 Minimally invasive TAC

At 10–12 weeks of age, (Nogo-A/B$^{f/f}$)Mlc2v-Cre+ and (Nogo-A/B$^{f/f}$)Mlc2v-Cre− (indicated as Nogo-A/B$^{f/f}$) were subjected to TAC or sham surgery as previously reported.[32] Briefly, mice were anaesthetized with ketamine/xylazine (100/5 mg/kg). After hair removal a horizontal incision was made at the level of second intercostal space. After retracting the thymus, the aortic arch was visualized by using a dissecting scope (Zeiss Discovery.V8 Stereo, Jena, Germany). A 7-0 nylon ligature was tied between the innominate and left common carotid artery with an overlying probe made from 26-gauge needle, which was then rapidly removed, leaving a discrete region of stenosis. Sham-operated animals underwent to the same surgical procedure without the ligation of the aorta.

## 2.3 Myriocin and chloroquine treatments of mice following TAC

At 10–12 weeks of age, (Nogo-A/B$^{f/f}$)Mlc2v-Cre+ and Nogo-A/B$^{f/f}$ were subjected to TAC surgery as previously reported.[32] (Nogo-A/B$^{f/f}$) Mlc2v-Cre+ and Nogo-A/B$^{f/f}$ mice were intraperitoneally injected with myriocin (My, 0.1 mg/kg, #M1177; Sigma, St Louis, MS, USA) in 0.4% fatty acid–free bovine serum albumin (BSA) in phosphate-buffered saline (PBS) or vehicle, as indicated. Mice were injected with My or vehicle at Days 1, 3, 5, 7, and 9 following TAC surgery (Day 0), and echocardiographic analysis was performed at 1 month post-TAC. In another set of experiments, TAC-operated (Nogo-A/B$^{f/f}$)Mlc2v-Cre+ and Nogo-A/B$^{f/f}$ mice were treated with My (0.1 mg/kg) at Days 1, 3, and 5. At Day 7 post-TAC, mice were sacrificed and CM isolated for Western blot (WB), reverse transcriptase-polymerase chain reaction (RT-PCR) analysis, and SL measurements.

In another set of experiments, at 7 days post-TAC, (Nogo-A/B$^{f/f}$) Mlc2v-Cre+ and Nogo-A/B$^{f/f}$ mice were treated with chloroquine (CQ; 10 mg/kg) or vehicle (water) and after 2 h mice were sacrificed and CM isolated for WB analysis.

## 2.4 Echocardiographic analysis

Cardiac dimensions and function were analysed by transthoracic echocardiogram using a Vevo 770 and 3100 Imaging Systems (VisualSonics, Toronto, ON, Canada).[32] Mice were lightly anaesthetized with inhaled isoflurane (2% in $O_2$). Left-ventricle M-mode was used, and all measurements were obtained from the averaged values of three consecutive cardiac cycles. Left-ventricle end-diastolic (LVDd) and end-systolic (LVDs) dimensions were measured from the M-mode traces, and fractional shortening (FS) was calculated as follows: [(LVDd—LVDs)/LVDd]. Diastolic measurements were taken at the point of maximum cavity dimension, and systolic measurements were made at the point of minimum cavity dimension, using the leading-edge method of the American Society of Echocardiography.[43]

## 2.5 Histological analysis of heart sections

Mice were sacrificed at different time points after TAC or sham surgery as indicated, and perfused with PBS via left ventricle at constant pressure of 80 mmHg. The hearts were fixed with 4% paraformaldehyde (PFA) overnight at 4°C. Some hearts were cut in half along the long axis and paraffin embedded. Following deparaffinization and rehydration, 5 µm thick heart sections were stained with haematoxylin and eosin (H&E). In another set of experiments, PFA-fixed hearts were incubated for 24 h in 30% sucrose solution at 4°C on rotation, then divided in three parts along the short axis (base, middle, and apex), incubated o.n. with 1:1 mixture of OCT/sucrose 30% and embedded in OCT. Myocardial section of 10 µm was used for immunofluorescent analysis. After permeabilization in 0.5% Triton X-100 in 5% BSA solution, frozen myocardial sections were incubated at 4°C o.n. with antibodies against Nogo-A/B (1:100, #AF-6034; R&D Systems, Minneapolis, MN, USA) and Nogo-A (1:100, #MAB3098; R&D Systems) in 5% BSA in PBS solution, followed by secondary antibodies in PBS solution, Alexa Fluor-555 donkey anti-sheep (1:200, #A21436; Invitrogen, Waltham, MA, USA) and Alexa Fluor 568-conjugated donkey anti-mouse IgG (1:200, #A10037; Invitrogen), and with fluorescein isothiocyanate (FITC)-conjugated wheat germ agglutinin (40 µg/mL; #L4895; Sigma) in PBS for 1 h at room temperature. Nuclei were stained with 4′,6-diamidino-2-phenylindole (DAPI). Z-stack immunofluorescence images were captured with Zeiss Axio Observer. Z1 microscope and deconvoluted with ZEN pro 2012 software (Carl Zeiss, Jena, Germany).

## 2.6 Flow cytometry analysis

Hearts were harvested, minced, and digested with Type I collagenase. Homogenates were filtered through a 40 µM filter to remove the CM. Non-CMs cell suspension was stained with the following antibodies (Biolegend, San Diego, CA, USA): CD45-APC (#103112), CD11b-FITC (#101206), CD3-APCCy7 (#100221 or #100330), CD19-PE (#152407 or #115508) CD4-PECy7 (#100421), CD4-PerCP/Cyanine5.5 (#100434), Ly6C-PECy7 (#128017), Ly6G-APCCy7 (#127623), Ly6G-Alexa Fluor 700 (#127622), CD64-PE (#139304). Samples were run on a BD Fortessa analyser (BD Biosciences, San Diego, CA, USA) and analysed with FlowJo software (BD Biosciences). Gating of populations and cell number calculations were performed as previously described.[44] The number of cells per heart of the indicated populations were obtained by multiplying the percentage of specific cell population with the total cellularity of the sample.

## 2.7 CM isolation from murine heart

CM were isolated from (Nogo-A/B$^{f/f}$)Mlc2v-Cre+ and Nogo-A/B$^{f/f}$ sham- and TAC-operated mice according to a modified version of AfCS Procedure Protocol PP00000125 as previously reported.[32] Briefly, the hearts were rapidly excised and cannulated, and perfused with AfCS perfusion buffer (mM: NaCl 113, KCl 4.7, $KH_2PO_4$ 0.6, $Na_2HPO_4$ 0.6, $MgSO_4$ 1.2, $NaHCO_3$ 12, $KHCO_3$ 10, HEPES 10, taurine 30, glucose 5.5, and 2,3-butandione monoxime (BDM) 10), for 5 min at a speed of 4 mL/min. Then with digestion buffer (1 mg/mL collagenase Type II and 50 µM $CaCl_2$ in AfCS) for 12–15 min. After enzymatic digestion of the heart (hearts appeared swollen, pale, and flaccid), the ventricles were excised and minced into small pieces in stop buffer (1 mg/mL collagenase Type 2, 15 mg/mL BSA and 50 µM $CaCl_2$ in AfCS) and bath at 37°C for 10 min. Pipets were used to gently dissociate the heart tissue until all large pieces were disaggregated. Cell suspensions were filtered with a 150 µm filter and CM were purified by three consecutive natural gravity sedimentations in AfCS buffer with increasing concentrations of $CaCl_2$, 100, 400, and 900 µM, respectively, of 15 min each, as recently reported by Li *et al.*[45]. CM were used for WB, RT-PCR, and SL analysis.

## 2.8 Real-time PCR analysis of gene expression

CM were isolated as aforementioned from the hearts of sham and TAC-operated (Nogo-A/B$^{f/f}$)Mlc2v-Cre+ and Nogo-A/B$^{f/f}$ mice at 7 days post-surgery. Total RNA was extracted according to the TRIzol reagent protocol (#15596026; ThermoFisher Scientific, Waltham, MA, USA). Maxima First Strand cDNA Synthesis Kit (#K1641; ThermoFisher Scientific) was used for the reverse transcription of 100 ng of RNA. For RT-PCR analysis, PowerUp™ SYBR™ Green Master Mix (#A25779; ThermoFisher Scientific, Waltham, MA, USA) and Applied Biosystems 7500 Fast RT-PCR system were used. Primer sets were: *Gapdh* (5′-AGGTCGGTGTGAACGGATTTG-3′ and 5′-TGTAGACCATGTAGTTGAGGTCA-3′), *Rtn4* (*Nogo-A/B*) (5′-GGTGCCTTGTTCAATGGTTT-3′ and 5′-ATTCTGCTTTGCGC TTCAAT-3′), *Tnnt2* (5′-TCCTGGCAGAGAGGAGGAAG-3′ and 5′-TGCAGGTCGAACTTCTCAGC-3′), *Nkx2.5* (5′-ACATTTTACCC GGGAGCCTA-3′ and 5′-GGCTTTGTCCAGCTCCACT-3′), *Fsp1* (5′-GATGAGCAACTTGGACAGCA-3′ and 5′-TGTGCGAAGAAGCC AGAGT-3′), *Cd45* (5′-CTTCAGTGGTCCCATTGTGGTG-3′ and 5′-TC AGACACCTCTGTCGCCTTAG-3′), *Cd31* (5′-CCAAAGCCAGTAG CATCATGGTC-3′ and 5′-GGATGGTGAAGTTGGCTACAGG-3′), *Ppara* (5′-GAGGGTTGAGCTCAGTCAGG-3′ and 5′-GGTCACCTACG AGTGGCATT-3′), *Glut4* (5′-ACTCTTGCCACACAGGCTCT-3′ and 5′-AATGGAGACTGATGCGCTCT-3′), *Cpt1b* (5′-GTCGCTTCTTCAA GGTCTGG-3′ and 5′-AAGAAAGCAGCACGTTCGAT-3′), *Cd36* (5′-TCCTCTGACATTTGCAGGTCTATC-3′ and 5′-AAAGGCA TTGGCTGGAAGAA-3′). Relative mRNA expression was calculated with the 2(−ΔΔCt) method, using *Gapdh* as housekeeping.[46]

## 2.9 WB analysis and co-immunoprecipitation (co-IP)

CM were isolated as described above from the hearts of sham and TAC-operated (Nogo-A/B$^{f/f}$)Mlc2v-Cre+ and Nogo-A/B$^{f/f}$ mice at 7 days, 1 and 3 months post-surgery. WB was performed as previously reported.[28] Protein extracts were prepared from isolated CM by using

radioimmunoprecipitation assay buffer (RIPA) buffer containing phosphatase (#04906845001; Roche, Basel, Switzerland) and protease (#11873580001; Roche) inhibitors. SDS-PAGE was performed using 50 μg of CM lysates. The following primary antibodies were used for WB analysis: ORMDL3 (#ABN417; Sigma), ceramide synthase 2 (CERS2; #20344-1-AP; Proteintech, Rosemont, IL, USA), SPTLC1 (#611304; BD Biosciences), SPTLC2 (#A11716; Abclonal, Woburn, MA, USA), LC3B and BECLIN-1 (#2775 and #3495; Cell Signaling Technology, Danvers, MA, USA), NOGO-A (#MAB3898; R&D Systems), NOGO-A/B (#AF6034; R&D Systems), PKCα/β (#BS-3531R; ThermoFisher Scientific), and GAPDH (ab181602; Abcam, Cambridge, United Kingdom).

To assess the interaction between SPT and NOGO-A, HEK293T cells were transfected with plasmids expressing SPTLC1 and MYC-NOGO-A. After 48 h, cells were lysed and NOGO-A was immunoprecipitated with antibody against MYC (#sc-40; Santa Cruz Biotechnology, Dallas, TX, USA) in modified RIPA buffer (50 mM Tris-HCl pH 7.2, 0.9% NaCl, 5.0 mM NaF, 1.0 mM $Na_3VO_4$, 1% NP40, and protease inhibitors) at 4°C o.n. The immune complexes were precipitated with protein A sepharose beads (Sigma) and size fractionated on SDS-PAGE gels. SPTLC1 co-immunoprecipitated with NOGO-A was detected with SPTLC1 antibody (#611304; BD Biosciences). To assess the interaction between SPT and Nogo-A *in vivo*, microsomal fractions from WT and Nogo-A/B$^{-/-}$ hearts were homogenized and resuspended in RIPA buffer. Nogo-A was immunoprecipitated using an antibody against Nogo-A (#MAB3898; R&D Systems) at 4°C o.n. The immune complexes were precipitated with Dynabeads protein G (#10003D; Invitrogen, for 1.5 h at 4°C) and size fractionated on SDS-PAGE gels.

## 2.10 SPT activity assay

CM were isolated as aforementioned from the hearts of sham and TAC-operated (Nogo-A/B$^{f/f}$)Mlc2v-Cre+ and Nogo-A/B$^{f/f}$ mice at 7 days, 1 and 3 months post-surgery. SPT activity was measured as previously described.[47] Briefly, CM were homogenized in SPT reaction buffer (0.1 M HEPES pH 8.3, 5 mM DTT, 2.5 mM EDTA pH 7.4, 50 μM pyridoxal 5′-phosphate). The assay was conducted in a volume of 0.1 mL composed by 200 μg of CM lysates, 0.45 μM [$^3$H]-serine (PerkinElmer, Shelton, CT, USA), 0.2 mM palmitoyl-CoA (#P9716; Sigma). After 15 min at 37°C, the reaction was stopped with $NaBH_4$ (5 mg/mL) that allows the conversion of the product 3-ketosphinganine into sphinganine (also known as dihydrosphingosine). Radiolabelled lipids were extracted by using a modified Bligh and Dyer's method,[48] dissolved in $CHCl_3$ and analysed by thin-layer chromatography. TLC plates were developed with chloroform, methanol, and ammonium hydroxide (65:25:4). [$^3$H]-Serine-labelled sphinganine was quantified using the RITA radioactivity TLC analyser (Raytest, Straubenhardt, Germany) and a [$^3$H]-serine calibration curve.

## 2.11 SL analysis by LC/MS/MS

CM were isolated from the hearts of sham and TAC-operated (Nogo-A/B$^{f/f}$)Mlc2v-Cre+ and Nogo-A/B$^{f/f}$ mice at 7 days, 1 and 3 months post-surgery. CM lysates in RIPA buffer were analysed for SL contents by LC/MS/MS at the Lipidomics Shared Resource at the Medical University of South Carolina as previously described.[32]

## 2.12 Diacylglycerol analysis by LC/MS/MS

CM were isolated from the hearts of TAC-operated (Nogo-A/B$^{f/f}$) Mlc2v-Cre+ and Nogo-A/B$^{f/f}$ mice at 7 days post-surgery. CM pellets were analysed for lipid contents by LC/MS/MS at the Proteomic and Metabolomic Core Facility at Weill Cornell Medicine and values were expressed per milligram of CM proteins.

## 2.13 Measurements of ROS production

CM from adult murine ventricles were isolated for ROS measurements.[49] Briefly, the heart was rapidly isolated, cannulated, and perfused with perfusion buffer (in mM: NaCl 120.4, KCl 14.7, $KH_2PO_4$ 0.6, $Na_2HPO_4$ 0.6, $MgSO_4$ 1.2, $NaHCO_3$ 4.6, HEPES 10, taurine 30, glucose 5.5, and BDM 10), for 5 min at a speed of 2.5 mL/min. Perfusion buffer was then replaced with digestion buffer (0.854 mg/mL Type 2 collagenase and 0.34 mg/mL proteinase XIV) and perfused for 10–15 min.[49] The heart was then teased into small pieces in stop buffer (perfusion buffer with 10% foetal bovine serum), filtered through a 100 μM nylon mesh, followed by centrifugation [1 min at 750 relative centrifugal force (RCF)]. The cells were successively resuspended in 10 mL stop buffer and $Ca^{2+}$ was gradually reintroduced to a final concentration of 1.2 mM.[50] After $Ca^{2+}$ reintroduction, cells were centrifuged (1 min at 750 RCF) and resuspended in imaging buffer (in mM: NaCl 116, KCl 5.4, $Na_2HPO_4$ 0.9, $MgSO_4$ 0.4, $CaCl_2$ 1.2, HEPES 20, taurine 20, glucose 10, and sodium pyruvate 5, pH = 7.4). Cells were plated onto 35 mm MatTek glass bottom dishes pre-coated for 2 h with 10 μg/mL laminin at RT and allowed to attach for 1 h.[51] For the assessment of cellular and mitochondrial ROS production, cells were incubated with 10 μM $H_2$DCF-DA[52] or with 5 μM MitoSOX,[50] respectively, for 10 min in imaging buffer. After washing out $H_2$DCF-DA or MitoSOX, cells were immediately visualized at the confocal microscope, as previously described.[50,53] At least five random wide fields of view were taken, each containing approximately 10–20 cells, and fluorescence measured with ImageJ; the same lasers and gains settings were used for all measurements.

## 2.14 Statistics

Data are expressed as mean ± SEM. Statistical analysis was performed using an unpaired two-tailed Student's *t* test, one-way analysis of variance (ANOVA), and two-way ANOVA with Tukey's multiple comparison test as indicated. Differences were considered statistically significant at $P \leq 0.05$. All tests were two sided. Statistical analyses were performed by using GraphPad Prism software (version 8.0).

# 3. Results

## 3.1 The loss of CM Nogo-A exacerbates pathological cardiac hypertrophy

Mlc2v-Cre[40,41] mice were used to excise Nogo-A in CM and investigate its role during pathological cardiac hypertrophy induced by TAC. The loss of Nogo-A did not affect the heart morphology in sham-operated (Nogo-A/B$^{f/f}$)Mlc2v-Cre+ mice compared with Nogo-A/B$^{f/f}$ (*Figure 1A* and *B*), suggesting that despite its expression in the atria and blood vessels of the heart,[32,54,55] Nogo is dispensable for cardiac development and homeostasis.

On the contrary, when mice were challenged with pressure overload, (Nogo-A/B$^{f/f}$)Mlc2v-Cre+ mice developed a severe dilated cardiomyopathy (*Figure 1A* and *B*) and enhanced heart weight/tibial length (HW/TL) ratios (*Figure 1C*) compared with Nogo-A/B$^{f/f}$. Similar results were obtained when Nogo-A was excised in CM by using Myh6-Cre[56] (see Supplementary material online, *Figure S1A and B*). The HW/TL ratios of Myh6-Cre+ mice was similar to Nogo-A/B$^{f/f}$ (see Supplementary

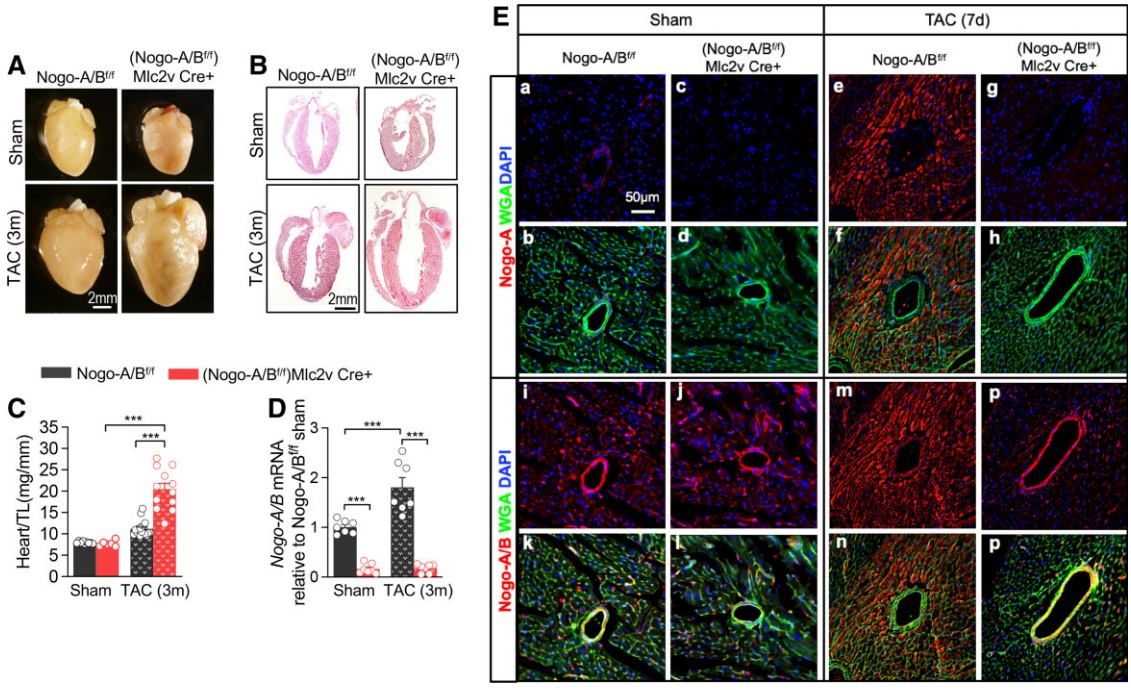


**Figure 1** The loss of cardiomyocytes Nogo-A exacerbates pathological cardiac hypertrophy. Representative images of (*A*) whole heart and (*B*) H&E staining of longitudinal heart sections of Nogo-A/B$^{f/f}$ and (Nogo-A/B$^{f/f}$)Mlc2v-Cre+ sham and 3-month TAC-operated mice. (*C*) Heart weight/tibial length (HW/TL) ratios of sham and 3-month TAC-operated mice. (*D*) Real-time (RT)-PCR for *Nogo-A/B* mRNA expression in CM isolated from sham and 7 days TAC-operated Nogo-A/B$^{f/f}$ and (Nogo-A/B$^{f/f}$)Mlc2v-Cre+ mice. GAPDH was used as housekeeping gene ($n = 7$ mice/group). (*E*) Immunofluorescence staining for Nogo-A/B and Nogo-A of myocardial sections from sham and TAC-operated Nogo-A/B$^{f/f}$ and (Nogo-A/B$^{f/f}$)Mlc2v-Cre+ mice. FITC-labelled wheat germ agglutinin (WGA) staining has been used to evidence cell membranes in myocardial sections. Nuclei are stained with DAPI. Data are expressed as mean ± SEM. ***$P \leq 0.001$; Statistical significance was determined by two-way ANOVA followed by Tukey's multiple comparison test.

material online, *Figure S1C*), arguing against a possible Cre-mediated toxicity[57] and attributing the excessive cardiac hypertrophy to the specific loss of Nogo-A.

RT-PCR analysis showed a robust efficiency in Cre-mediated excision of Nogo-A in CM of pressure overloaded hearts (*Figure 1D*). Previously, we demonstrated that Nogo-A, but not Nogo-B, is transiently expressed in CM after pressure overload.[32] At 7 days post-TAC, immunofluorescent staining of myocardial sections showed the expression of Nogo-A in CM of Nogo-A/B$^{f/f}$ mice, whereas was undetectable in most of the CM of (Nogo-A/B$^{f/f}$)Mlc2v-Cre+ myocardial sections (*Figure 1E*, Panels e, f vs. g, h; and see Supplementary material online, *Figure S2*). Nogo-A/B knockout hearts were used as negative controls (see Supplementary material online, *Figure S3*). Considering that only CM were positively stained for Nogo-A, the staining of blood vessels of both (Nogo-A/B$^{f/f}$)Mlc2v-Cre+ and Nogo-A/B$^{f/f}$ hearts with the antibody against Nogo-A/B represented the isoform Nogo-B (*Figure 1E*, Panel m vs. p). These data showed that following TAC, Nogo-A is expressed in CM and protects the heart from severe pathological cardiac hypertrophy under sustained haemodynamic stress.

## 3.2 Cardiac Nogo-A protects from HF and mortality following pressure overload

Echocardiographic analysis of (Nogo-A/B$^{f/f}$)Mlc2v-Cre+ mice revealed a severe HF compared with Nogo-A/B$^{f/f}$ post-TAC, with increasing LVDd and LVDs, and reduced FS (*Figure 2A–D*). Similar outcomes were obtained by excising Nogo-A in CM with the Myh6-Cre approach (see Supplementary material online, *Figure S1D–F*).

Severe HF in absence of Nogo resulted in ca. 50% mortality of (Nogo-A/B$^{f/f}$)Mlc2v-Cre+ mice at 12 weeks post-TAC vs. controls (*Figure 2E*). Several studies pointed out the critical role of inflammation in the pathogenesis of heart diseases,[58] with macrophages and T lymphocytes mediating essential roles in the progression to HF during pressure overload.[59] Flow cytometry analysis for CD45$^+$ leucocytes, monocytes, macrophages, neutrophils, CD4$^+$ T cell, CD4$^-$ CD3$^+$ T cell, and B-cell populations was increased to the same extent in (Nogo-A/B$^{f/f}$)Mlc2v-Cre+ and Nogo-A/B$^{f/f}$ hearts at 7 days post-TAC (*Figure 2F–L*) compared with Nogo-A/B$^{f/f}$ sham, suggesting that the loss of Nogo-A in CM did not impact myocardial inflammation following pressure overload.

## 3.3 Nogo-A refrains ceramide accrual in CM under haemodynamic stress

We discovered that endothelial Nogo-B acts as negative regulator of SL *de novo* biosynthesis, by inhibiting the rate-limiting enzyme SPT.[29] Thus, we assessed whether Nogo-A was able to interact with SPT and regulate its activity. To this end, MYC-tagged NOGO-A and SPTLC1, an SPT subunit, were co-expressed in HEK293T cells. SPTLC1 co-immunoprecipitated with Nogo-A (*Figure 3A*). To corroborate this interaction *in vivo*, we used myocardial lysates at 7 days post-TAC, when Nogo-A is expressed, as well as brain lysates, expressing Nogo-A in physiological conditions.[60] Nogo-A and SPTLC1

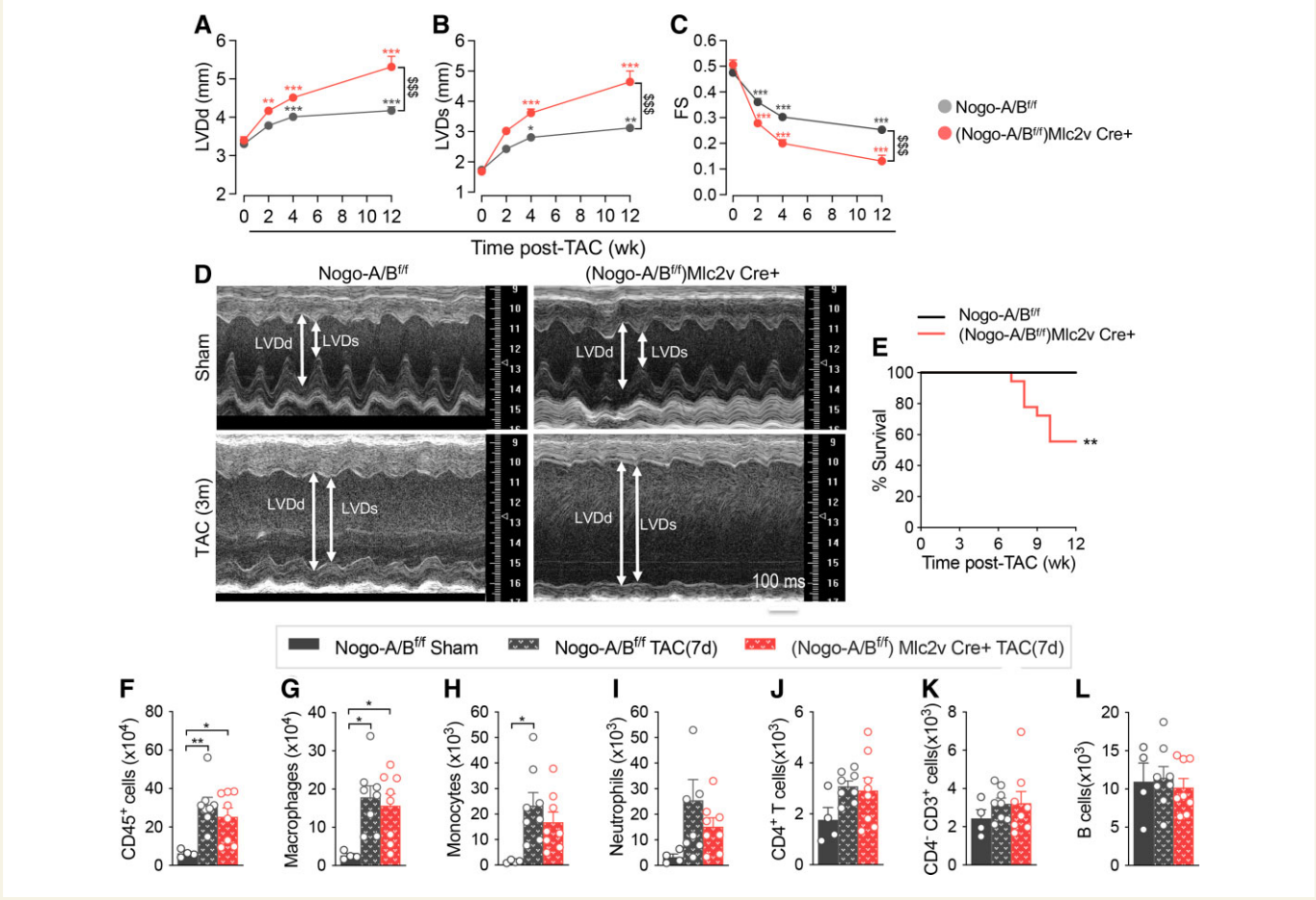


**Figure 2** The absence of Nogo-A in CM worsen heart failure and decreases survival rate. Echocardiographic analysis of sham- and TAC-operated Nogo-A/B$^{f/f}$ ($n = 14$) and (Nogo-A/B$^{f/f}$)Mlc2v-Cre+ ($n = 12$) mice at different time points. (*A*) Left-ventricle end-diastolic diameter (LVDd), (*B*) LV end-systolic diameter (LVDs), (*C*) fractional shortening (FS) measured at baseline and 2, 4, and 12 weeks after TAC. (*D*) Representative images of LV serial echocardiography. (*E*) Survival curve of Nogo-A/B$^{f/f}$ ($n = 16$) and (Nogo-A/B$^{f/f}$)Mlc2v-Cre+ ($n = 18$) post-TAC. Survival analysis was performed by the Kaplan–Meier method, and between-group differences in survival were evaluated by using the Gehan–Breslow–Wilcoxon test. Flow cytometry analysis of inflammatory cells in non-CM cell suspension from the hearts of sham-operated Nogo-A/B$^{f/f}$ mice ($n = 4$), Nogo-A/B$^{f/f}$ and (Nogo-A/B$^{f/f}$)Mlc2v-Cre+ at 7 days post-TAC ($n = 8$ mice/group). Total number of: (*F*) CD45$^+$ haematopoietic cells; (*G*) CD45$^+$, CD64$^{Lo}$, Ly6C$^{Hi}$ monocytes; (*H*) CD45$^+$, Ly6C$^{Lo}$, Ly6G$^-$, CD64$^{Hi}$ macrophages; (*I*) CD45$^+$, CD64$^-$, Ly6C$^{Med}$, Ly6G$^{Hi}$ neutrophils; (*J*) CD4$^+$ CD3$^+$ T cells; (*K*) CD4$^-$ CD3$^+$ T cells; and (*L*) CD19$^+$ B cells. Data are expressed as mean ± SEM. *$P \leq 0.05$; **$P \leq 0.01$. In *A–C*, *** is statistic vs. time 0 of the same genotype, and $$$ is statistic between the genotypes. Statistical significance was determined by two-way ANOVA followed by Tukey's multiple comparison test (*A–C*) and one-way ANOVA (*F–L*)

co-immunoprecipitated from heart (*Figure 3B*) and brain (see Supplementary material online, *Figure S4A*) lysates, validating the interaction of SPTLC1-Nogo-A in an *in vivo* setting. Of note, Nogo proteins are phosphorylated,[61–63] hence the two bands. In myocardial lysates treated with λ-phosphatase, the upper band disappears, suggesting that it corresponds to phosphorylated Nogo-A (see Supplementary material online, *Figure S4B*).

To investigate the impact of Nogo-A on SL metabolism, we measured SPT activity and ceramide levels in CM isolated from (Nogo-A/B$^{f/f}$)Mlc2v-Cre+ and Nogo-A/B$^{f/f}$ mice sham and at 7 days, 1 and 3 months post-TAC. First, the purity of CM was assessed by RT-PCR analyses. *Tnnt2*, and *Nkx2.5,* lineage markers for CM, were significantly enriched in the CM compared with the non-CM fractions (*Figure 3C*), while *Fsp1*, *Cd45*, and *Cd31*, lineage markers for fibroblasts, inflammatory, and endothelial cells (ECs) respectively, were markedly down-regulated (*Figure 3D–F*), indicating very low levels of these cell types. WB analysis showed that NOGO-A expression was increased in CM at 7 days and 1 month post-TAC, whereas it was undetectable at 3 months post-TAC (*Figure 3G*). The loss of NOGO-A did not up-regulate SPT activity in CM of sham mice (*Figure 3H*). However, following pressure overload, CM SPT activity was significantly elevated in absence of NOGO-A at 7 days and 1 month post-TAC vs. Nogo-A/B$^{f/f}$ (*Figure 3H*), suggesting that CM NOGO-A refrains the increase of ceramide *de novo* biosynthesis following pressure overload.

Notably, SPT activity was not changed in CM of Nogo-A/B$^{f/f}$ at different time points post-TAC (7 days, 1 and 3 months) compared with sham (*Figure 3H*), suggesting that NOGO-A exerts a brake on stress-induced SPT activity.

Similarly, when NOGO-A was expressed, CM ceramides were not changed at any time point post-TAC (*Figure 3I–L*), whereas they were elevated in CM lacking NOGO-A 7 days and 1 month but not at 3 months post-TAC (*Figure 3I–L* and see Supplementary material online, *Figure S5A*). As expected, significant changes occurred in very long-chain ceramides (C20:0-Cer to C24:1-Cer), the most abundant (*Figure 3J–L*).

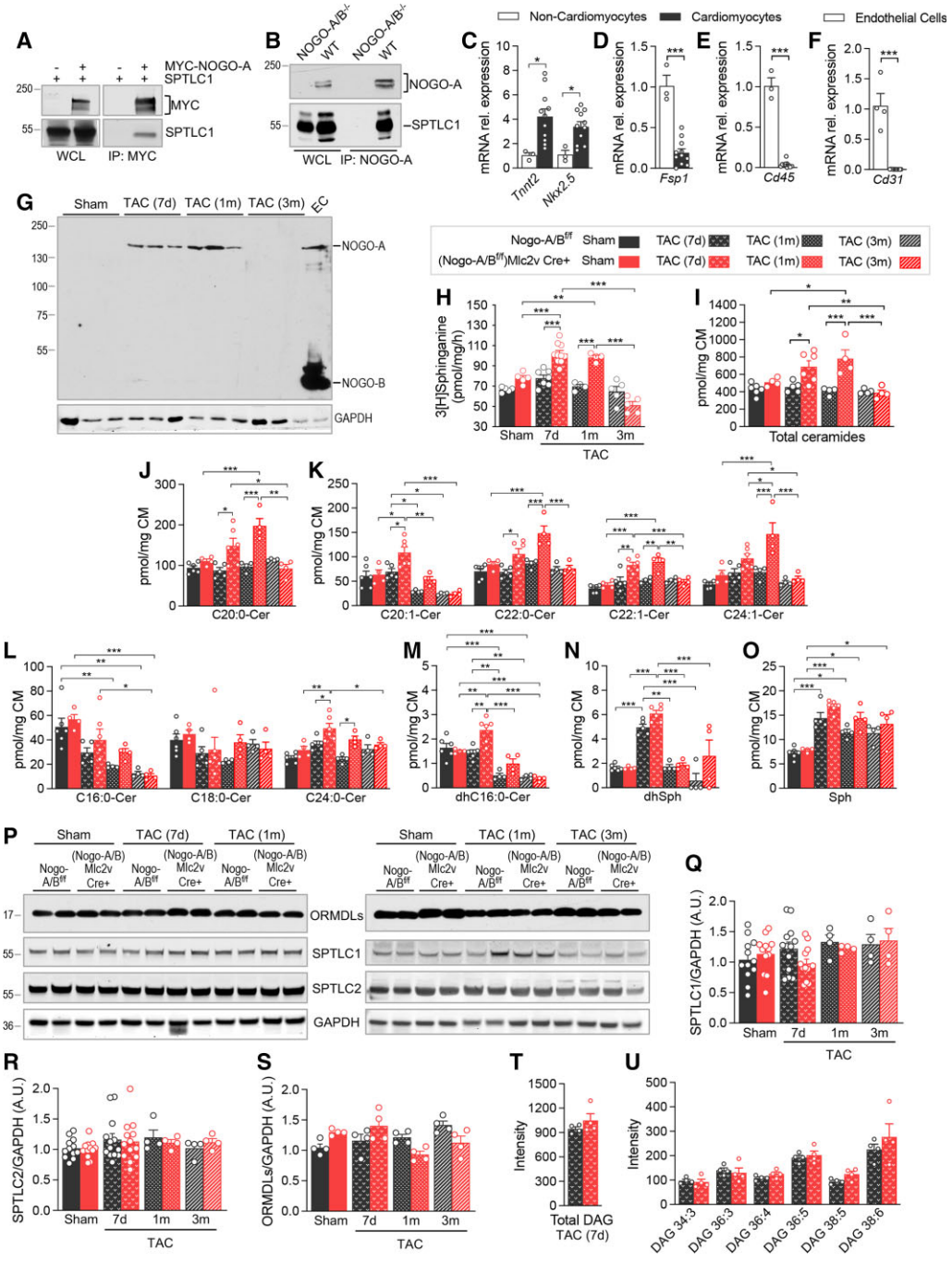


**Figure 3** Nogo-A interacts with SPT and regulates ceramide *de novo* biosynthesis in cardiomyocytes. (*A*) Western blot (WB) analysis of transfected SPTLC1 and MYC-NOGO-A in HEK293T whole cell lysate (WCL) and after co-immunoprecipitation (co-IP) with anti-MYC antibody. (*B*) WB analysis of Nogo-A and SPTLC1 in NOGO-A/B$^{-/-}$ and WT myocardial microsomes, in WCL and after co-IP with anti-NOGO-A antibody. RT-PCR for (*C*) *Tnnt2* and *Nkx2.5*, (*D*) *Fsp1*, and (*E*) *Cd45* mRNA expression in CM vs. non-CM fractions. (*F*) RT-PCR for *Cd31* mRNA expression in CM fraction vs. endothelial cells (ECs). (*G*) WB analysis of NOGO-A in CM isolated from Nogo-A/B$^{f/f}$ and (Nogo-A/B$^{f/f}$)Mlc2v-Cre+ mice sham, 7 days, 1 and 3 months post-TAC. EC lysate has been used as positive control for NOGO-B expression. (*H*) SPT activity in CM isolated from Nogo-A/B$^{f/f}$ [sham $n=5$; TAC (7d) $n=7$; TAC (1m) $n=4$; TAC (3m) $n=5$] and (Nogo-A/B$^{f/f}$)Mlc2v-Cre+ [sham $n=5$; TAC (7d) $n=10$; TAC (1m) $n=4$; TAC (3m) $n=5$] mice. (*I*) Total ceramides, (*J–L*) specific ceramides, (*M*) C16:0-dihydro ceramide (dhC16:0-cer), (*N*) dihydrosphingosine (dhSph), and (*O*) sphingosine (Sph) measured in CM isolated from Nogo-A/B$^{f/f}$ [sham $n=6$; TAC (7d) $n=5$, TAC (1m) $n=4$, TAC (3m) $n=4$] and (Nogo-A/B$^{f/f}$)Mlc2v-Cre+ [sham $n=4$; TAC (7d) $n=6$, TAC (1m) $n=4$, TAC (3m) $n=4$] mice. (*P*) WB analysis and (*Q–S*) relative quantification of ORMDLs, SPTLC1, and SPTLC2 expression, performed on CM isolated from sham and TAC(7d)-operated Nogo-A/B$^{f/f}$ and (Nogo-A/B$^{f/f}$)Mlc2v-Cre+ mice ($n \geq 4$/group). GAPDH was used as housekeeping. (*T*) Total diacylglycerols (DAGs) and (*U*) specific DAG measured in Nogo-A/B$^{f/f}$ and (Nogo-A/B$^{f/f}$)Mlc2v-Cre+ ($n=4$/group) CM at 7 days post-TAC. Data are expressed as mean ± SEM. *$P \leq 0.05$; **$P \leq 0.01$; ***$P \leq 0.001$. Statistical significance was determined by unpaired *t* test (*C–F*, *T–U*), and two-way ANOVA followed by Tukey's multiple comparison test (*H–O*, *Q–S*).

Interestingly, longitudinal increase in SPT activity and ceramides in CM correlated with NOGO-A expression.

To understand the molecular mechanisms underlying stress-induced SPT activity, we assessed the expression of known components of the SPT complex. WB analysis showed no difference in SPTLC1 and SPTLC2 expression in CM of sham- and TAC-operated mice (*Figure 3P–R*). ORMDL proteins (ORMDL1,2,3) down-regulate the activity of SPT.[64] WB analysis on CM showed no difference in ORMDLs expression in all conditions (*Figure 3P* and *S*). CERS2 is accountable for the synthesis of the very long-chain ceramides, abundant in CM (i.e. C22:0-, C24:0-, and C24:1-ceramide), and has been reported to be up-regulated in the ischaemic hearts of mice and humans.[11] However, WB analysis in CM showed no changes in all conditions (see Supplementary material online, *Figure S5B and C*). The small subunits of SPT, ssSPTa and ssSPTb, interact with SPT and function as activators.[65,66] Thus, we assessed the mRNA levels of *Sssptа/b* by RT-PCR. In CM lacking Nogo-A, *Sssptb* but not *Sssptа* expression was significantly decreased 7 days post-TAC, thus most likely changes in ssSPTa and ssSPTb expression are not accountable for the increased SPT activity CM lacking Nogo-A post-TAC (see Supplementary material online, *Figure S5D and E*). Of note, changes in mRNA not necessarily correspond to protein levels. For instance, *Sptlc1* and *Sptlc2* mRNA were significantly down-regulated in CM of Nogo-A/B$^{f/f}$ mice at 7 days post-TAC (see Supplementary material online, *Figure S5F and G*), but not at protein levels, which were unchanged (*Figure 3P–R*).

In addition to ceramides, diacylglycerols (DAGs), activators of PKC enzymes,[67] are often found increased in the failing hearts.[23] However, DAG levels were no different at 7 days post-TAC in CM with and without Nogo (*Figure 3T–U*), nor were different the levels of PKCα/β (see Supplementary material online, *Figure S6*), thus arguing against a role of DAG in the severe pathological hypertrophy of (Nogo-A/B$^{f/f}$) Mlc2v-Cre+.

## 3.4 CM Nogo-A deficiency exacerbates HF by inhibiting protective autophagy

Autophagy is an essential cellular mechanism for the removal of damaged cytoplasmic components.[68] Haemodynamic stress activates cardiac autophagy.[24,69] Whether autophagy plays a beneficial or detrimental role in the heart exposed to pressure overload has been under debate.[24,69,70] Recently, an elegant study of Shirakabe and colleagues demonstrated that autophagy is transiently activated by pressure overload and exerts a critical cardioprotective function.[70] To test whether Nogo-A brake on ceramide production preserves autophagy, the expression of LC3B-II and BECLIN-1, markers of autophagy, were assessed. LC3B-II and BECLIN-1 were significantly up-regulated in Nogo-A/B$^{f/f}$ but not in (Nogo-A/B$^{f/f}$)Mlc2v-Cre+ CM at 7 days post-TAC (*Figure 4A–D*). To assess the autophagic flux, at 7 days post-TAC mice were treated with CQ, inhibitor of the autophagosome-lysosome fusion.[71] WB analysis showed that CQ treatment increased LC3B-II and BECLIN-1 levels in Nogo-A/B$^{f/f}$ but not in (Nogo-A/B$^{f/f}$) Mlc2v-Cre+ CM (*Figure 4E–G*). These data suggests that in absence of Nogo-A the accrual of ceramides in CM suppressed the autophagic flux and the early onset of protective autophagy, therefore exacerbating pathological cardiac hypertrophy. To corroborate these data, we used human CM (hCM) in culture treated with isoproterenol (ISO) as *in vitro* model of CM hypertrophy. Contrary to *in vivo*, hCM in culture express both Nogo-B and Nogo-A in basal conditions (see Supplementary material online, *Figure S7A*), therefore this *in vitro* system does not recapitulate the regulation of SPT by Nogo-A in CM *in vivo* during pressure overload. On the contrary, the silencing of *Cers2*, synthetizing the very long-chain C22:0-, C24:0-, and C24:1-ceramide, most abundant in CM, decreased ceramide levels and boosted autophagy in basal and ISO-stimulated conditions (see Supplementary material online, *Figure S7B and C*), supporting the inhibitory role of ceramides on autophagy. Altogether, these data suggest that Nogo-A preserves the onset of 'protective' autophagy during pressure overload by refraining ceramide biosynthesis.

Another key feature of HF pathophysiology is oxidative stress,[50,72–74] which is exacerbated by ceramide accrual.[75] Nogo-A deletion did not affect cellular and mitochondrial reactive oxygen species (ROS) formation in CM of sham-operated mice. On the contrary, both mitochondrial and cellular ROS were significantly higher in CM lacking Nogo-A at 7 days post-TAC vs. Nogo-A/B$^{f/f}$ (*Figure 4H* and *I*), suggesting that in absence of Nogo-A ceramide accrual exacerbates ROS production contributing to worsen cardiac hypertrophy and dysfunction.

## 3.5 Inhibition of the ceramide *de novo* biosynthesis with myriocin restores CM autophagy and prevents HF in absence of Nogo-A

To demonstrate that in absence of Nogo-A ceramide accrual suppresses autophagy in pressure overloaded CM, (Nogo-A/B$^{f/f}$)Mlc2v-Cre+ and Nogo-A/B$^{f/f}$ mice received myriocin treatment (My, 0.1 mg/kg i.p., an SPT inhibitor) at Days 1, 3, and 5 following TAC surgery. Strikingly, My was able to fully restore LC3B-II and BECLIN-1 expression in (Nogo-A/B$^{f/f}$)Mlc2v-Cre+ CM to Nogo-A/B$^{f/f}$ levels at 7 days post-TAC (*Figure 5A–C*). In another experimental setting, mice were treated with My (0.1 mg/kg, i.p.) at Days 1, 3, 5, 7, and 9 post-surgery. At 1 month post-TAC, FS and cardiac hypertrophy were significantly improved in (Nogo-A/B$^{f/f}$)Mlc2v-Cre+ mice treated with My compared with vehicle (*Figure 5D–H*).

Cardiac hypertrophy and HF induced by pressure overload are exacerbated in mice lacking *Ppara*,[76] *Glut4*,[77] *Cpt1b*,[78] and *Cd36*,[79] underlying the importance of metabolic homeostasis for cardiac health. Thus, we have investigated the impact of *Nogo-A* deletion on glucose and lipid metabolism. At 7 days post-TAC, consistent with the worst cardiac hypertrophy, *Ppara*, *Glut4*, *Cpt1B*, and *Cd36* expressions were increased in Nogo-A/B$^{f/f}$ but not in (Nogo-A/B$^{f/f}$)Mlc2v-Cre+ (*Figure 5I*). Interestingly, My treatment restored their mRNA levels to Nogo-A/B$^{f/f}$ mice post-TAC (*Figure 5I*), in line with ceramide levels. Altogether, these data confirm that in absence of NOGO-A, the accrual of ceramides in CM suppresses beneficial autophagy, enhances the mitochondrial and cellular oxidative stress, and down-regulates the expression of cardioprotective metabolic genes, hence exacerbating the pathological cardiac hypertrophy.

# 4. Discussion

Despite growing evidence implicating ceramides in HF, mechanisms underlying the derangement of ceramide metabolism and its pathological implications remain poorly understood. Multiple clinical studies have identified plasma ceramides as independent predictors of major cardiovascular events. C16:0-, C18:0-, and C24:1-ceramide positively associated with cardiovascular disease incidence,[80] cardiovascular secondary events,[81,82] and mortality,[14,16,83] whereas C24:0-ceramide negatively correlated with cardiovascular mortality.[14,16,83] Myocardial

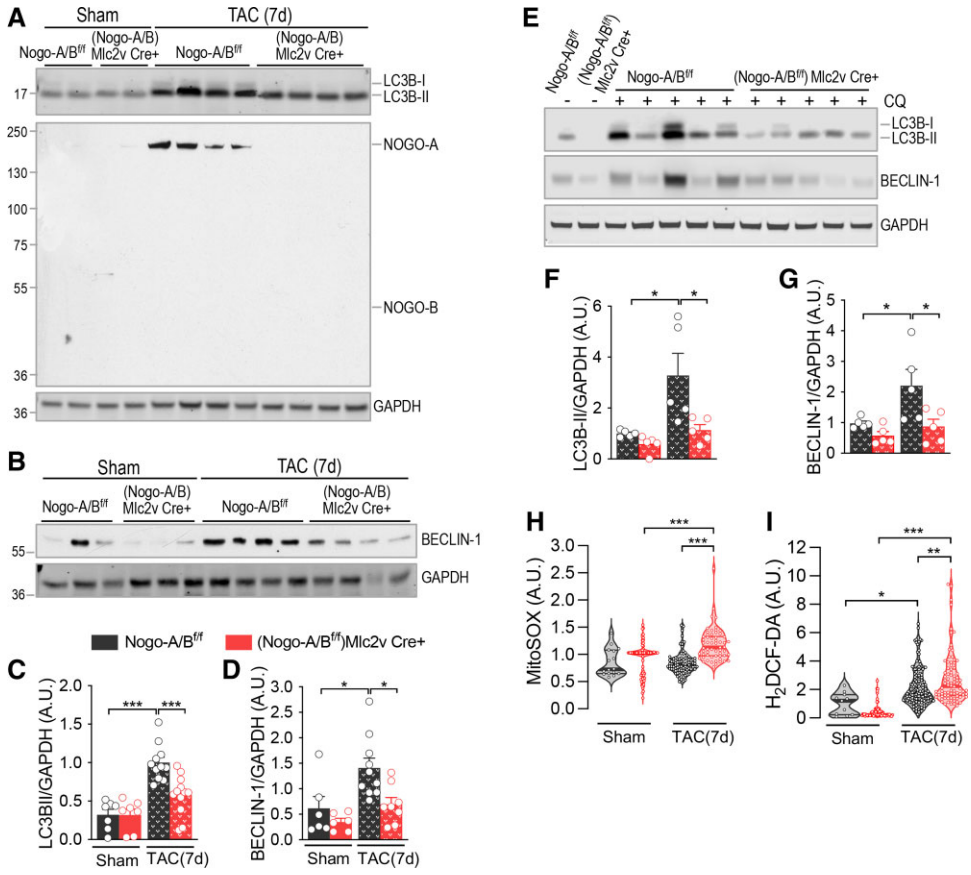


**Figure 4** Cardiomyocyte Nogo-A preserves beneficial autophagy by refraining ceramide *de novo* biosynthesis. (*A*) WB analysis of LC3B-II and NOGO-A/B and (*B*) BECLIN-1 expression in CM from Nogo-A/B$^{f/f}$ and (Nogo-A/B$^{f/f}$)Mlc2v-Cre+ mice. GAPDH was used as housekeeping. (*C*) Quantification of LC3B-II expression in Nogo-A/B$^{f/f}$ [sham $n=7$; TAC (7d) $n=11$] and (Nogo-A/B$^{f/f}$)Mlc2v-Cre+ [sham $n=7$; TAC (7d) $n=12$] CM. (*D*) Quantification of BECLIN-1 expression in Nogo-A/B$^{f/f}$ [sham $n=6$; TAC (7d) $n=10$] and (Nogo-A/B$^{f/f}$)Mlc2v-Cre+ [sham $n=6$; TAC (7d) $n=8$] CM. (*E*) WB analysis of LC3B-II and BECLIN-1 expression in CM from Nogo-A/Bf/f and (Nogo-A/B$^{f/f}$)Mlc2v-Cre+ mice at 7 days post-TAC, with or without CQ. GAPDH was used as housekeeping. Quantification of (*F*) LC3B-II and (*G*) BECLIN-1 expression in Nogo-A/B$^{f/f}$ and (Nogo-A/B$^{f/f}$)Mlc2v-Cre+ CM ($n=5$). Quantification of (*H*) mitochondrial ROS in Nogo-A/B$^{f/f}$ [sham $n=16$; TAC (7d) $n=91$] and (Nogo-A/B$^{f/f}$)Mlc2v-Cre+ [sham $n=109$; TAC (7d) $n=59$] CM and (*I*) cellular ROS in Nogo-A/B$^{f/f}$ [sham $n=11$; TAC (7d) $n=153$] and (Nogo-A/B$^{f/f}$)Mlc2v-Cre+ [sham $n=77$; TAC (7d) $n=86$] CM. Data are expressed as mean ± SEM. *$P\leq0.05$; **$P\leq0.01$; ***$P\leq0.001$. Statistical significance was determined by two-way ANOVA followed by Tukey's multiple comparison test.

ceramides are reported elevated in models of lipotoxic[2,18–20] and ischaemic cardiomyopathy,[11,21] in animals and humans. Hence, in recent years the interest in understanding the molecular mechanisms regulating ceramide biosynthesis in the heart has intensified.

Here, we investigated the impact of pressure overload on ceramide metabolism and signalling specifically in CM. We discovered that Nogo-A restrains ceramide *de novo* biosynthesis via SPT in CM following pressure overload, and preserves 'beneficial autophagy,' mitochondrial functions and metabolic adaptation, to protect the heart from failure. Following TAC, Nogo-A is expressed in CM and prevents ceramide from accrual. Our data are in agreement with the study of He *et al.*,[78] reporting that myocardial ceramides were not changed at early time point post-TAC. Goldenberg *et al.*[84] demonstrated an increase in myocardial ceramides at 14 weeks post-TAC. It is noteworthy to mention that whereas we measured ceramides specifically in CM at different time points post-TAC, both studies reported ceramide levels in myocardial tissues, including other cell types than CM (i.e. inflammatory cells, fibroblasts, and vascular cells), that can contribute to the changes in myocardial ceramides.

Pathologically, mice-lacking CM Nogo-A manifested severe dilated cardiomyopathy and mortality, underlying a protective role of Nogo-A in CM. Previous studies from our group and others have demonstrated the expression of Nogo in pathological hearts. Myocardial expression of Nogo-A and Nogo-B is increased following TAC,[32] with Nogo-A specifically confined to CM.[32] Gramolini *et al.*[35] reported Nogo up-regulation in a phospholamban mutant mouse model of dilated cardiomyopathy. Up-regulation of *Rtn4* gene has been described in different animal models of dilated cardiomyopathy and in HF in humans[32,35–39]; hence, Nogo has been regarded as potential biomarker of heart diseases. Yet, Nogo functions in CM are largely unknown.

Here, we discovered that the functional role of Nogo-A in CM is to limit ceramide *de novo* biosynthesis via SPT inhibition, and preserve 'beneficial' autophagy, mitochondrial functions and metabolic adaptation to pressure overload, thus limiting the development of pathological cardiac hypertrophy. That Nogo-A refrains from hypertrophy *in vivo* is consistent with the *in vitro* study of Li *et al.*[85] describing an enhanced hypertrophy in neonatal rat CM following Nogo knockdown.

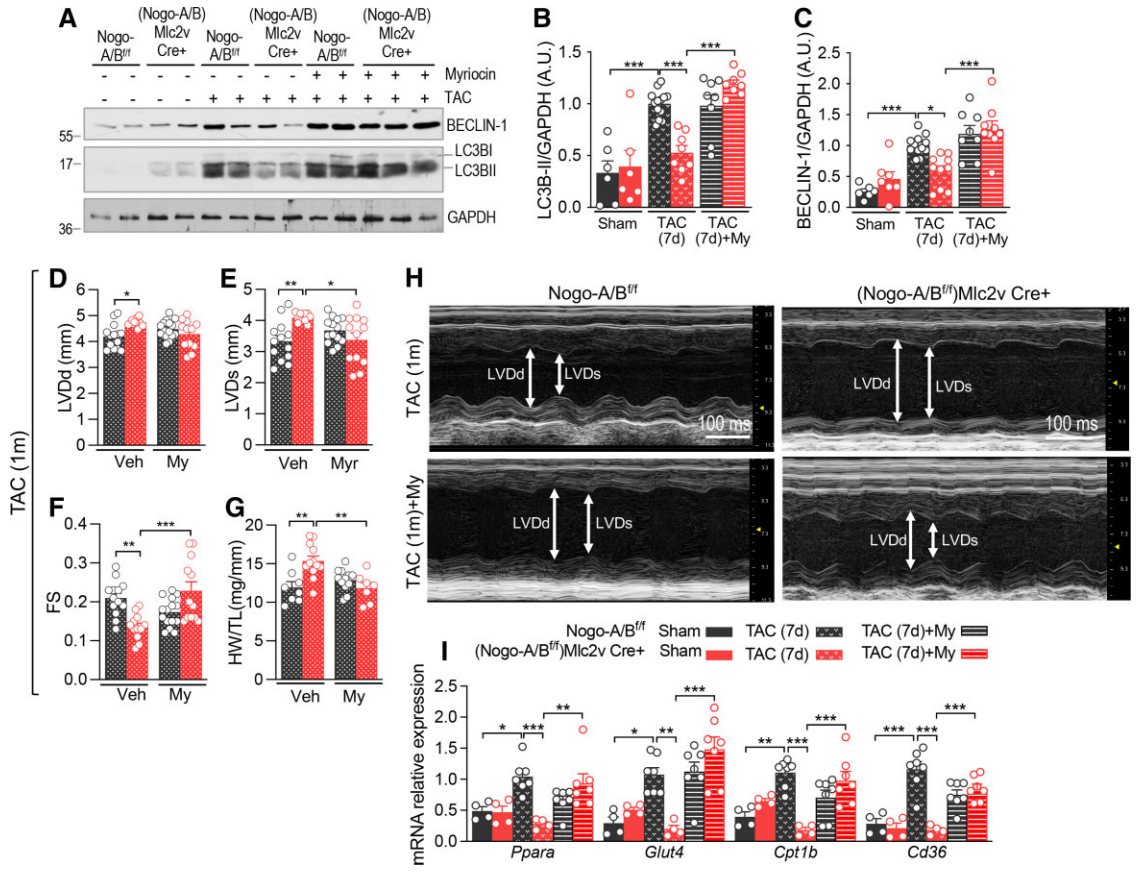


**Figure 5** Inhibition of the ceramide *de novo* biosynthesis with myriocin restores CM autophagy and prevents HF in absence of Nogo-A. (*A*) WB analysis and quantification of (*B*) LC3B-II and (*C*) BECLIN-1 expression in CM from Nogo-A/B$^{f/f}$ [sham $n=6$, TAC (7d) $n=12$, TAC (7d + My) $n=8$] and (Nogo-A/B$^{f/f}$)Mlc2v-Cre+ [sham $n=6$, TAC (7d) $n=8$, TAC (7d + My) $n=8$] mice. GAPDH was used as housekeeping. Echocardiographic analysis of vehicle- and My-treated TAC-operated Nogo-A/B$^{f/f}$ (vehicle $n=13$; My $n=15$) and (Nogo-A/B$^{f/f}$)Mlc2v-Cre+ (vehicle $n=12$; My $n=12$) mice. (*D*) LVDd, (*E*) LVDs, (*F*) FS, and (*G*) HW/TL ratios of vehicle- and My-treated Nogo-A/B$^{f/f}$ (vehicle $n=8$; My $n=12$) and (Nogo-A/B$^{f/f}$)Mlc2v-Cre+ mice (vehicle $n=12$, My $n=7$) measured at 1 month post-TAC. (*H*) Representative images of LV serial echocardiography. (*I*) RT-PCR for *Ppara*, *Glut4*, *Cpt1B*, and *Cd36* in CM isolated from Nogo-A/B$^{f/f}$ [sham $n=4$, TAC (7d) $n=7$; TAC (7d)+My $n=7$] and (Nogo-A/B$^{f/f}$)Mlc2v-Cre+ [sham $n=4$, TAC (7d) $n=4$; TAC (7d)+My $n=7$] mice. Data are expressed as mean ± SEM. *$P\leq0.05$; **$P\leq0.01$; ***$P\leq0.001$. Statistical significance was determined by two-way ANOVA followed by Tukey's multiple comparison test.

Interestingly, contrary to the beneficial role of Nogo-A in CM, endothelial Nogo-B is detrimental in HF[32] and hypertension.[29] Following pressure overload, mice lacking endothelial Nogo-B are protected from permeability, inflammation, and pathological cardiac hypertrophy via an up-regulation of S1P-S1PR1 signalling.[32] S1P is a potent activator of endothelial nitric oxide synthase and enhancer of the barrier function, thus limiting cardiac inflammation and damage. The divergent roles for the same protein in different cell types of the heart have been reported before.[86] For instance, cardiac SMAD3 plays divergent roles in CM vs. fibroblast, therefore leads to opposite outcomes in myocardial infarction models.[86]

Elevated ceramides are known to contribute to the dysregulation of cellular functions, including cell growth, differentiation, senescence, and apoptosis.[87] Myocardial accrual of ceramides has been reported in lipotoxic cardiomyopathy[2] and ischaemic conditions in animals and humans.[11,88,89] The *de novo* ceramide pathway has been implicated in the pathology of lipotoxic cardiomyopathy[2,19] and myocardial infarction.[11,88] This is the first study to identify a regulatory mechanism of ceramide *de novo* biosynthesis in CM during pressure overload and its impact on HF. Under stress conditions, Nogo-A down-regulates SPT in CM and prevents the intracellular rise of ceramides, considered detrimental for the heart.[19,22,28] It is noteworthy to mention that the genetic deletion of Nogo-A does not change SPT activity in healthy CM (*Figure 3H*), which is not surprising considering that in physiological conditions CM do not express Nogo-A[32] (*Figures 1* and *3*). However, SPT activity was significantly up-regulated in CM lacking Nogo-A at 7 days and 1 month post-TAC. Interestingly, we found no changes in the expression of known components of the SPT complex (*Figure 3P–S* and see Supplementary material online, *Figure 5D–G*). These findings suggest that under haemodynamic stress a 'yet-to-be identified' regulator of SPT complex (i.e. an activator) might be expressed and up-regulates SPT activity in CM. The deletion of Nogo-A removes the brake on SPT and reveals the increase of SPT activity in stressed CM. Further studies are needed to elucidate molecular changes of SPT complex in these conditions.

Mechanistically, our data showed that Nogo-A refrains ceramide from accrual and therefore preserves cardiac autophagy. Previous studies have implicated ceramides in the control of autophagy.[7] Cardiac

autophagy is of fundamental importance. It occurs constitutively at low levels to maintain cellular homeostasis and is up-regulated in pressure overload,[69,70] limiting the accumulation of the misfolded protein, mitochondrial dysfunction, and oxidative stress.[25] We investigated autophagy as one of the potential mechanisms in ceramide-dependent cardiac dysfunction. The loss of Nogo-A dramatically suppressed autophagy in CM and was not increased by CQ treatment, suggesting that the autophagic flux was impaired (*Figure 4E–G*). This finding was further corroborated by pharmacological treatment of mice lacking CM Nogo-A with myriocin, an inhibitor of SPT, which was able to restore protective autophagy in CM exposed to haemodynamic stress (*Figure 5A–C*), and protect the heart from failing (*Figure 5D–H*). The finding that ceramide suppresses CM autophagy was further corroborated by *Cers2* silencing in a human CM cell line, resulting in significant up-regulation of autophagy at baseline and following isoproterenol stimulation (see Supplementary material online, *Figure S7*). Our data agree with the study of Spassieva *et al.*,[90] showing that the disruption of ceramide synthesis by CERS2 leads to autophagy.

In neuronal cells, Nogo-A does not contribute to ER stress-associated apoptosis.[91] Furthermore, the unfolded protein response, including ATF6, IRE1, PERK pathways, is not affected by the loss of Nogo.[92] Therefore, it seems that Nogo does not have a main impact on the ER stress-associated apoptosis. Our data strongly implicate an important role of Nogo in cardiac autophagy via ceramide regulation. When ceramide is increased to 'pathological levels' can shut down completely autophagy, therefore impeding the removal of misfolded proteins and damaged organelles in CM, events that contribute to the cellular damage.

Russo and colleagues[19] showed that a diet rich in saturated fatty acid or CM treatment with myristate induces autophagy and hypertrophy via the up-regulation of ceramide, specifically C14:0-ceramide, the least abundant in CM (*Figure 3* and see Supplementary material online, *Figure S5A*). Our findings demonstrate that in absence of Nogo-A, ceramide accrual suppresses the early onset of 'beneficial autophagy' in CM of pressure overloaded hearts. A possible explanation for this discordance could be that divergent mechanisms may underlie the pathogenesis of different heart conditions (i.e. lipotoxic vs. pressure-overload cardiomyopathy), and that both excessive and deficient autophagy are deleterious.[25] However, that the loss of Nogo-A suppresses the early onset of 'beneficial autophagy' resulting in severe cardiomyopathy agrees with the study of Shirakabe and colleagues,[70] who elegantly demonstrated that following pressure overload, there is a transient activation of autophagy exerting cardioprotective functions. One limitation of our study is the lack of intervention on the autophagic flux to impact cardiac hypertrophy.

The requirement for Nogo-A down-regulation of ceramide *de novo* biosynthesis in CM extends beyond autophagy to include defects in mitochondrial functions and metabolic gene expression that manifest in its absence. Different studies demonstrated a direct effect of ceramides on the respiratory chain of isolated mitochondria leading to the formation of ROS.[93,94] Oxidative stress is another key feature in HF pathophysiology.[50,72–74] In line with these findings, in CM lacking Nogo-A, there is a significant increase in oxidative stress at 7 days post-TAC, which is known to contribute to HF.[95]

Elevation in 1,2-DAG, a potent activator of PKC isoforms, plays an important role HF.[23] However, in pressure overloaded hearts, the levels of DAG were not affected by the loss of Nogo-A in CM, arguing against a potential role of DAG in the severe dilated cardiomyopathy observed in (Nogo-A/B$^{f/f}$)Mlc2v-Cre+ mice.

The suppression of PPARα,[76,96] GLUT4,[77] CPT1B,[78] and CD36[79,97] metabolic genes exacerbates HF induced by pressure overload, underlying the importance of metabolic homeostasis to preserve heart function. Interestingly, in absence of Nogo-A, the expression of these genes was significantly suppressed, and rescued by myriocin, suggesting that Nogo-A-ceramide signalling can impart a 'protective' transcriptional signature in CM under haemodynamic stress. Further studies are necessary to unveil the mechanisms governing these transcriptional changes. A limitation of this study is the lack of Nogo-A gain of function.

Finally, our characterization of cardiac Nogo-A function also provides a framework for investigating whether alterations in Nogo-A activity and SL metabolism play a role also in other pathological conditions. SNPs in RTN4 correlate with coronary artery disease,[98] schizophrenia,[99,100] and cancer.[101,102] Our findings that Nogo-A protects the heart against pressure overload-induced hypertrophy and failure, by preserving the 'beneficial autophagy' via ceramide, suggests also that Nogo dysregulation of SL metabolism may have a causal role in other pathological conditions beyond HF.

# Supplementary material

Supplementary material is available at *Cardiovascular Research* online.

## Acknowledgements

The authors thank Drs Jessica Gambardella, PhD and Urna Kansakar, PhD for technical support and advice.

**Conflict of interest:** None declared.

## Funding

This work was supported by the National Heart, Lung, and Blood Institute of the National Institutes of Health grant R01 HL126913 and R01 HL152195 to A. Di Lorenzo.

## Data availability

The data underlying this article are available in the article and in its online supplementary material.

## References

1. Benjamin EJ, Muntner P, Alonso A, Bittencourt MS, Callaway CW, Carson AP, Chamberlain AM, Chang AR, Cheng S, Das SR, Delling FN, Djousse L, Elkind MSV, Ferguson JF, Fornage M, Jordan LC, Khan SS, Kissela BM, Knutson KL, Kwan TW, Lackland DT, Lewis TT, Lichtman JH, Longenecker CT, Loop MS, Lutsey PL, Martin SS, Matsushita K, Moran AE, Mussolino ME, O'Flaherty M, Pandey A, Perak AM, Rosamond WD, Roth GA, Sampson UKA, Satou GM, Schroeder EB, Shah SH, Spartano NL, Stokes A, Tirschwell DL, Tsao CW, Turakhia MP, VanWagner LB, Wilkins JT, Wong SS, Virani SS, American Heart Association Council on Epidemiology and Prevention Statistics Committee and Stroke Statistics Subcommittee. Heart disease and stroke statistics 2019. Update: a report from the American Heart Association. *Circulation* 2019;**139**:e56–e528.
2. Park TS, Hu Y, Noh HL, Drosatos K, Okajima K, Buchanan J, Tuinei J, Homma S, Jiang XC, Abel ED, Goldberg IJ. Ceramide is a cardiotoxin in lipotoxic cardiomyopathy. *J Lipid Res* 2008;**49**:2101–2112.
3. Drosatos K, Schulze PC. Cardiac lipotoxicity: molecular pathways and therapeutic implications. *Curr Heart Fail Rep* 2013;**10**:109–121.
4. Doenst T, Nguyen TD, Abel ED. Cardiac metabolism in heart failure: implications beyond ATP production. *Circ Res* 2013;**113**:709–724.
5. Hannun YA, Obeid LM. The ceramide-centric universe of lipid-mediated cell regulation: stress encounters of the lipid kind. *J Biol Chem* 2002;**277**:25847–25850.
6. Yang J, Yu Y, Sun S, Duerksen-Hughes PJ. Ceramide and other sphingolipids in cellular responses. *Cell Biochem Biophys* 2004;**40**:323–350.
7. Young MM, Kester M, Wang HG. Sphingolipids: regulators of crosstalk between apoptosis and autophagy. *J Lipid Res* 2013;**54**:5–19.
8. Spijkers LJA, van den Akker RFP, Janssen BJA, Debets JJ, De Mey JGR, Stroes ESG, van den Born BJH, Wijesinghe DS, Chalfant CE, MacAleese L, Eijkel GB, Heeren RMA,

Alewijnse AE, Peters SLM. Hypertension is associated with marked alterations in sphingolipid biology: a potential role for ceramide. *PLoS One* 2011; **6**:e21817.
9. Lemaitre RN, Jensen PN, Hoofnagle A, McKnight B, Fretts AM, King IB, Siscovick DS, Psaty BM, Heckbert SR, Mozaffarian D, Sotoodehnia N. Plasma ceramides and sphingomyelins in relation to heart failure risk. *Circ Heart Fail* 2019;**12**:e005708.
10. Yu J, Pan W, Shi R, Yang T, Li Y, Yu G, Bai Y, Schuchman EH, He X, Zhang G. Ceramide is upregulated and associated with mortality in patients with chronic heart failure. *Can J Cardiol* 2015;**31**:357–363.
11. Ji R, Akashi H, Drosatos K, Liao X, Jiang H, Kennel PJ, Brunjes DL, Castillero E, Zhang X, Deng LY, Homma S, George IJ, Takayama H, Naka Y, Goldberg IJ, Schulze PC. Increased de novo ceramide synthesis and accumulation in failing myocardium. *JCI Insight* 2017;**2**:e82922.
12. Chaurasia B, Summers SA. Ceramides - lipotoxic inducers of metabolic disorders. *Trends Endocrinol Metab* 2015;**26**:538–550.
13. van de Weijer T, Schrauwen-Hinderling VB, Schrauwen P. Lipotoxicity in type 2 diabetic cardiomyopathy. *Cardiovasc Res* 2011;**92**:10–18.
14. Laaksonen R, Ekroos K, Sysi-Aho M, Hilvo M, Vihervaara T, Kauhanen D, Suoniemi M, Hurme R, Marz W, Scharnagl H, Stojakovic T, Vlachopoulou E, Lokki ML, Nieminen MS, Klingenberg R, Matter CM, Hornemann T, Juni P, Rodondi N, Raber L, Windecker S, Gencer B, Pedersen ER, Tell GS, Nygard O, Mach F, Sinisalo J, Luscher TF. Plasma ceramides predict cardiovascular death in patients with stable coronary artery disease and acute coronary syndromes beyond LDL-cholesterol. *Eur Heart J* 2016;**37**:1967–1976.
15. Meeusen JW, Donato LJ, Bryant SC, Baudhuin LM, Berger PB, Jaffe AS. Plasma ceramides. *Arterioscler Thromb Vascu Biol* 2018;**38**:1933–1939.
16. Peterson LR, Xanthakis V, Duncan MS, Gross S, Friedrich N, Volzke H, Felix SB, Jiang H, Sidhu R, Nauck M, Jiang X, Ory DS, Dorr M, Vasan RS, Schaffer JE. Ceramide remodeling and risk of cardiovascular events and mortality. *J Am Heart Assoc* 2018;**7**:e007931.
17. Park TS, Goldberg IJ. Sphingolipids, lipotoxic cardiomyopathy, and cardiac failure. *Heart Fail Clin* 2012;**8**:633–641.
18. Son NH, Park TS, Yamashita H, Yokoyama M, Huggins LA, Okajima K, Homma S, Szabolcs MJ, Huang LS, Goldberg IJ. Cardiomyocyte expression of PPARgamma leads to cardiac dysfunction in mice. *J Clin Invest* 2007;**117**:2791–2801.
19. Russo SB, Baicu CF, Van Laer A, Geng T, Kasiganesan H, Zile MR, Cowart LA. Ceramide synthase 5 mediates lipid-induced autophagy and hypertrophy in cardiomyocytes. *J Clin Invest* 2012;**122**:3919–3930.
20. Walls SM, Cammarato A, Chatfield DA, Ocorr K, Harris GL, Bodmer R. Ceramide-protein interactions modulate ceramide-associated lipotoxic cardiomyopathy. *Cell Rep* 2018;**22**:2702–2715.
21. Bielawska AE, Shapiro JP, Jiang L, Melkonyan HS, Piot C, Wolfe CL, Tomei LD, Hannun YA, Umansky SR. Ceramide is involved in triggering of cardiomyocyte apoptosis induced by ischemia and reperfusion. *Am J Pathol* 1997;**151**:1257–1263.
22. Law BA, Liao X, Moore KS, Southard A, Roddy P, Ji R, Szulc Z, Bielawska A, Schulze PC, Cowart LA. Lipotoxic very-long-chain ceramides cause mitochondrial dysfunction, oxidative stress, and cell death in cardiomyocytes. *FASEB J* 2018;**32**:1403–1416.
23. Schulze PC, Drosatos K, Goldberg IJ. Lipid use and misuse by the heart. *Circ Res* 2016;**118**:1736–1751.
24. Nakai A, Yamaguchi O, Takeda T, Higuchi Y, Hikoso S, Taniike M, Omiya S, Mizote I, Matsumura Y, Asahi M, Nishida K, Hori M, Mizushima N, Otsu K. The role of autophagy in cardiomyocytes in the basal state and in response to hemodynamic stress. *Nat Med* 2007;**13**:619–624.
25. Sciarretta S, Maejima Y, Zablocki D, Sadoshima J. The role of autophagy in the heart. *Annu Rev Physiol* 2018;**80**:1–26.
26. Yamaguchi O, Taneike M, Otsu K. Cooperation between proteolytic systems in cardiomyocyte recycling. *Cardiovasc Res* 2012;**96**:46–52.
27. Eisenberg T, Abdellatif M, Schroeder S, Primessnig U, Stekovic S, Pendl T, Harger A, Schipke J, Zimmermann A, Schmidt A, Tong M, Ruckenstuhl C, Dammbrueck C, Gross AS, Herbst V, Magnes C, Trausinger G, Narath S, Meinitzer A, Hu Z, Kirsch A, Eller K, Carmona-Gutierrez D, Buttner S, Pietrocola F, Knittelfelder O, Schrepfer E, Rockenfeller P, Simonini C, Rahn A, Horsch M, Moreth K, Beckers J, Fuchs H, Gailus-Durner V, Neff F, Janik D, Rathkolb B, Rozman J, de Angelis MH, Moustafa T, Haemmerle G, Mayr M, Willeit P, von Frieling-Salewsky M, Pieske B, Scorrano L, Pieber T, Pechlaner R, Willeit J, Sigrist SJ, Linke WA, Muhlfeld C, Sadoshima J, Dengjel J, Kiechl S, Kroemer G, Sedej S, Madeo F. Cardioprotection and lifespan extension by the natural polyamine spermidine. *Nat Med* 2016;**22**:1428–1438.
28. Lee SY, Kim JR, Hu Y, Khan R, Kim SJ, Bharadwaj KG, Davidson MM, Choi CS, Shin KO, Lee YM, Park WJ, Park IS, Jiang XC, Goldberg IJ, Park TS. Cardiomyocyte specific deficiency of serine palmitoyltransferase subunit 2 reduces ceramide but leads to cardiac dysfunction. *J Biol Chem* 2012;**287**:18429–18439.
29. Cantalupo A, Zhang Y, Kothiya M, Galvani S, Obinata H, Bucci M, Giordano FJ, Jiang XC, Hla T, Di Lorenzo A. Nogo-B regulates endothelial sphingolipid homeostasis to control vascular function and blood pressure. *Nat Med* 2015;**21**:1028–1037.
30. Sasset L, Di Lorenzo A. Sphingolipid metabolism and signaling in endothelial cell functions. *Adv Exp Med Biol* 2022;**1372**:87–117.
31. Di Lorenzo A, Manes TD, Davalos A, Wright PL, Sessa WC. Endothelial reticulon-4B (Nogo-B) regulates ICAM-1-mediated leukocyte transmigration and acute inflammation. *Blood* 2011;**117**:2284–2295.
32. Zhang Y, Huang Y, Cantalupo A, Azevedo PS, Siragusa M, Bielawski J, Giordano FJ, Di Lorenzo A. Endothelial Nogo-B regulates sphingolipid biosynthesis to promote pathological cardiac hypertrophy during chronic pressure overload. *JCI Insight* 2016;**1**:e85484.
33. Huber AB, Weinmann O, Brösamle C, Oertle T, Schwab ME. Patterns of Nogo mRNA and protein expression in the developing and adult rat and after CNS lesions. *J Neurosci* 2002;**22**:3553–3567.
34. Ortega A, Rosello-Lleti E, Tarazon E, Molina-Navarro MM, Martinez-Dolz L, Gonzalez-Juanatey JR, Lago F, Montoro-Mateos JD, Salvador A, Rivera M, Portoles M, Long D. Endoplasmic reticulum stress induces different molecular structural alterations in human dilated and ischemic cardiomyopathy. *PLoS One* 2014;**9**:e107635.
35. Gramolini AO, Kislinger T, Alikhani-Koopaei R, Fong V, Thompson NJ, Isserlin R, Sharma P, Oudit GY, Trivieri MG, Fagan A, Kannan A, Higgins DG, Huedig H, Hess G, Arab S, Seidman JG, Seidman CE, Frey B, Perry M, Backx PH, Liu PP, MacLennan DH, Emili A. Comparative proteomics profiling of a phospholamban mutant mouse model of dilated cardiomyopathy reveals progressive intracellular stress responses. *Mol Cell Proteomics* 2008;**7**:519–533.
36. Bullard TA, Protack TL, Aguilar F, Bagwe S, Massey HT, Blaxall BC. Identification of Nogo as a novel indicator of heart failure. *Physiol Genomics* 2008;**32**:182–189.
37. Sarkey JP, Chu M, McShane M, Bovo E, Ait Mou Y, Zima AV, de Tombe PP, Kartje GL, Martin JL. Nogo-A knockdown inhibits hypoxia/reoxygenation-induced activation of mitochondrial-dependent apoptosis in cardiomyocytes. *J Mol Cell Cardiol* 2011;**50**:1044–1055.
38. Sasagawa S, Nishimura Y, Okabe S, Murakami S, Ashikawa Y, Yuge M, Kawaguchi K, Kawase R, Okamoto R, Ito M, Tanaka T. Downregulation of GSTK1 is a common mechanism underlying hypertrophic cardiomyopathy. *Front Pharmacol* 2016;**7**:162.
39. Toischer K, Rokita AG, Unsold B, Zhu W, Kararigas G, Sossalla S, Reuter SP, Becker A, Teucher N, Seidler T, Grebe C, Preuss L, Gupta SN, Schmidt K, Lehnart SE, Kruger M, Linke WA, Backs J, Regitz-Zagrosek V, Schafer K, Field LJ, Maier LS, Hasenfuss G. Differential cardiac remodeling in preload versus afterload. *Circulation* 2010;**122**:993–1003.
40. Chen J, Kubalak SW, Minamisawa S, Price RL, Becker KD, Hickey R, Ross J Jr, Chien KR. Selective requirement of myosin light chain 2v in embryonic heart function. *J Biol Chem* 1998; **273**:1252–1256.
41. Minamisawa S, Gu Y, Ross J Jr, Chien KR, Chen J. A post-transcriptional compensatory pathway in heterozygous ventricular myosin light chain 2-deficient mice results in lack of gene dosage effect during normal cardiac growth or hypertrophy. *J Biol Chem* 1999; **274**:10066–10070.
42. Zheng B, Ho C, Li S, Keirstead H, Steward O, Tessier-Lavigne M. Lack of enhanced spinal regeneration in Nogo-deficient mice. *Neuron* 2003;**38**:213–224.
43. Mitchell C, Rahko PS, Blauwet LA, Canaday B, Finstuen JA, Foster MC, Horton K, Ogunyankin KO, Palma RA, Velazquez EJ. Guidelines for performing a comprehensive transthoracic echocardiographic examination in adults: recommendations from the American Society of Echocardiography. *J Am Soc Echocardiogr* 2019;**32**:1–64.
44. Chia JJ, Zhu T, Chyou S, Dasoveanu DC, Carballo C, Tian S, Magro CM, Rodeo S, Spiera RF, Ruddle NH, McGraw TE, Browning JL, Lafyatis R, Gordon JK, Lu TT. Dendritic cells maintain dermal adipose-derived stromal cells in skin fibrosis. *J Clin Invest* 2016;**126**:4331–4345.
45. Li H, Liu C, Bao M, Liu W, Nie Y, Lian H, Hu S. Optimized Langendorff perfusion system for cardiomyocyte isolation in adult mouse heart. *J Cell Mol Med* 2020;**24**:14619–14625.
46. Livak KJ, Schmittgen TD. Analysis of relative gene expression data using real-time quantitative PCR and the 2(-Delta Delta C(T)) method. *Methods* 2001;**25**:402–408.
47. Williams RD, Wang E, Merrill AH Jr. Enzymology of long-chain base synthesis by liver: characterization of serine palmitoyltransferase in rat liver microsomes. *Arch Biochem Biophys* 1984; **228**:282–291.
48. Bligh EG, Dyer WJ. A rapid method of total lipid extraction and purification. *Can J Biochem Physiol* 1959;**37**:911–917.
49. Morelli MB, Shu J, Sardu C, Matarese A, Santulli G. Cardiosomal microRNAs are essential in post-infarction myofibroblast phenoconversion. *Int J Mol Sci* 2019;**21**:201.
50. Santulli G, Xie W, Reiken SR, Marks AR. Mitochondrial calcium overload is a key determinant in heart failure. *Proc Natl Acad Sci U S A* 2015;**112**:11389–11394.
51. Amgalan D, Garner TP, Pekson R, Jia XF, Yanamandala M, Paulino V, Liang FG, Corbalan JJ, Lee J, Chen Y, Karagiannis GS, Sanchez LR, Liang H, Narayanagari SR, Mitchell K, Lopez A, Margulets V, Scarlata M, Santulli G, Asnani A, Peterson RT, Hazan RB, Condeelis JS, Oktay MH, Steidl U, Kirshenbaum LA, Gavathiotis E, Kitsis RN. A small-molecule allosteric inhibitor of BAX protects against doxorubicin-induced cardiomyopathy. *Nat Cancer* 2020;**1**:315–328.
52. Xie W, Santulli G, Reiken SR, Yuan Q, Osborne BW, Chen BX, Marks AR. Mitochondrial oxidative stress promotes atrial fibrillation. *Sci Rep* 2015;**5**:11427.
53. Tang XH, Gambardella J, Jankauskas SS, Wang X, Santulli G, Gudas LJ, Levi R. A retinoic acid receptor beta 2 agonist improves cardiac function in a heart failure model. *J Pharmacol Exp Ther* 2021;**379**:182–190.
54. Acevedo L, Yu J, Erdjument-Bromage H, Miao RQ, Kim JE, Fulton D, Tempst P, Strittmatter SM, Sessa WC. A new role for Nogo as a regulator of vascular remodeling. *Nat Med* 2004;**10**:382–388.
55. Nath AK, Krauthammer M, Li P, Davidov E, Butler LC, Copel J, Katajamaa M, Oresic M, Buhimschi I, Buhimschi C, Snyder M, Madri JA. Proteomic-based detection of a protein cluster dysregulated during cardiovascular development identifies biomarkers of congenital heart defects. *PLoS One* 2009;**4**:e4221.

56. Agah R, Frenkel PA, French BA, Michael LH, Overbeek PA, Schneider MD. Gene recombination in postmitotic cells. Targeted expression of Cre recombinase provokes cardiac-restricted, site-specific rearrangement in adult ventricular muscle in vivo. *J Clin Invest* 1997;**100**:169–179.
57. Pugach EK, Richmond PA, Azofeifa JG, Dowell RD, Leinwand LA. Prolonged Cre expression driven by the alpha-myosin heavy chain promoter can be cardiotoxic. *J Mol Cell Cardiol* 2015;**86**:54–61.
58. Mann DL. Inflammatory mediators and the failing heart: past, present, and the foreseeable future. *Circ Res* 2002;**91**:988–998.
59. Martini E, Kunderfranco P, Peano C, Carullo P, Cremonesi M, Schorn T, Carriero R, Termanini A, Colombo FS, Jachetti E, Panico C, Faggian G, Fumero A, Torracca L, Molgora M, Cibella J, Pagiatakis C, Brummelman J, Alvisi G, Mazza EMC, Colombo MP, Lugli E, Condorelli G, Kallikourdis M. Single-cell sequencing of mouse heart immune infiltrate in pressure overload-driven heart failure reveals extent of immune activation. *Circulation* 2019;**140**:2089–2107.
60. GrandPre T, Nakamura F, Vartanian T, Strittmatter SM. Identification of the Nogo inhibitor of axon regeneration as a reticulon protein. *Nature* 2000;**403**:439–444.
61. Rousseau S, Peggie M, Campbell DG, Nebreda AR, Cohen P. Nogo-B is a new physiological substrate for MAPKAP-K2. *Biochem J* 2005;**391**:433–440.
62. Schweigreiter R, Stasyk T, Contarini I, Frauscher S, Oertle T, Klimaschewski L, Huber LA, Bandtlow CE. Phosphorylation-regulated cleavage of the reticulon protein Nogo-B by caspase-7 at a noncanonical recognition site. *Proteomics* 2007;**7**:4457–4467.
63. Yokoyama K, Tezuka T, Hoshina N, Nakazawa T, Yamamoto T. Phosphorylation at Tyr-694 of Nogo-A by Src-family kinases. *Biochem Biophys Res Commun* 2006;**349**:1401–1405.
64. Breslow DK, Collins SR, Bodenmiller B, Aebersold R, Simons K, Shevchenko A, Ejsing CS, Weissman JS. Orm family proteins mediate sphingolipid homeostasis. *Nature* 2010;**463**:1048–1053.
65. Harmon JM, Bacikova D, Gable K, Gupta SD, Han G, Sengupta N, Somashekarappa N, Dunn TM. Topological and functional characterization of the ssSPTs, small activating subunits of serine palmitoyltransferase. *J Biol Chem* 2013;**288**:10144–10153.
66. Han G, Gupta SD, Gable K, Niranjanakumari S, Moitra P, Eichler F, Brown RH Jr, Harmon JM, Dunn TM. Identification of small subunits of mammalian serine palmitoyltransferase that confer distinct acyl-CoA substrate specificities. *Proc Natl Acad Sci U S A* 2009; **106**:8186–8191.
67. Dorn GW II, Force T. Protein kinase cascades in the regulation of cardiac hypertrophy. *J Clin Invest* 2005;**115**:527–537.
68. Levine B, Klionsky DJ. Development by self-digestion: molecular mechanisms and biological functions of autophagy. *Dev Cell* 2004;**6**:463–477.
69. Zhu H, Tannous P, Johnstone JL, Kong Y, Shelton JM, Richardson JA, Le V, Levine B, Rothermel BA, Hill JA. Cardiac autophagy is a maladaptive response to hemodynamic stress. *J Clin Invest* 2007;**117**:1782–1793.
70. Shirakabe A, Zhai P, Ikeda Y, Saito T, Maejima Y, Hsu CP, Nomura M, Egashira K, Levine B, Sadoshima J. Drp1-dependent mitochondrial autophagy plays a protective role against pressure overload-induced mitochondrial dysfunction and heart failure. *Circulation* 2016;**133**:1249–1263.
71. Mauthe M, Orhon I, Rocchi C, Zhou X, Luhr M, Hijlkema KJ, Coppes RP, Engedal N, Mari M, Reggiori F. Chloroquine inhibits autophagic flux by decreasing autophagosome-lysosome fusion. *Autophagy* 2018;**14**:1435–1455.
72. Lee J, Giordano S, Zhang J. Autophagy, mitochondria and oxidative stress: cross-talk and redox signalling. *Biochem J* 2012;**441**:523–540.
73. Tsutsui H, Kinugawa S, Matsushima S. Oxidative stress and heart failure. *Am J Physiol Heart Circ Physiol* 2011;**301**:H2181–H2190.
74. Takimoto E, Kass DA. Role of oxidative stress in cardiac hypertrophy and remodeling. *Hypertension* 2007;**49**:241–248.
75. Funai K, Summers SA, Rutter J. Reign in the membrane: how common lipids govern mitochondrial function. *Curr Opin Cell Biol* 2020;**63**:162–173.
76. Smeets PJH, Teunissen BEJ, Willemsen PHM, van Nieuwenhoven FA, Brouns AE, Janssen BJA, Cleutjens JPM, Staels B, van der Vusse GJ, van Bilsen M. Cardiac hypertrophy is enhanced in PPAR alpha-/- mice in response to chronic pressure overload. *Cardiovasc Res* 2008;**78**:79–89.
77. Wende AR, Kim J, Holland WL, Wayment BE, O'Neill BT, Tuinei J, Brahma MK, Pepin ME, McCrory MA, Luptak I, Halade GV, Litwin SE, Abel ED. Glucose transporter 4-deficient hearts develop maladaptive hypertrophy in response to physiological or pathological stresses. *Am J Physiol Heart Circ Physiol* 2017;**313**:H1098–H1108.
78. He L, Kim T, Long Q, Liu J, Wang P, Zhou Y, Ding Y, Prasain J, Wood PA, Yang Q. Carnitine palmitoyltransferase-1b deficiency aggravates pressure overload-induced cardiac hypertrophy caused by lipotoxicity. *Circulation* 2012;**126**:1705–1716.
79. Sung MM, Byrne NJ, Kim TT, Levasseur J, Masson G, Boisvenue JJ, Febbraio M, Dyck JR. Cardiomyocyte-specific ablation of CD36 accelerates the progression from compensated cardiac hypertrophy to heart failure. *Am J Physiol Heart Circ Physiol* 2017;**312**:H552–H560.
80. de Carvalho LP, Tan SH, Ow GS, Tang Z, Ching J, Kovalik JP, Poh SC, Chin CT, Richards AM, Martinez EC, Troughton RW, Fong AY, Yan BP, Seneviratna A, Sorokin V, Summers SA, Kuznetsov VA, Chan MY. Plasma ceramides as prognostic biomarkers and their arterial and myocardial tissue correlates in acute myocardial infarction. *JACC Basic Transl Sci* 2018;**3**:163–175.
81. Hilvo M, Meikle PJ, Pedersen ER, Tell GS, Dhar I, Brenner H, Schottker B, Laaperi M, Kauhanen D, Koistinen KM, Jylha A, Huynh K, Mellett NA, Tonkin AM, Sullivan DR, Simes J, Nestel P, Koenig W, Rothenbacher D, Nygard O, Laaksonen R. Development and validation of a ceramide- and phospholipid-based cardiovascular risk estimation score for coronary artery disease patients. *Eur Heart J* 2020;**41**:371–380.
82. Wang DD, Toledo E, Hruby A, Rosner BA, Willett WC, Sun Q, Razquin C, Zheng Y, Ruiz-Canela M, Guasch-Ferre M, Corella D, Gomez-Gracia E, Fiol M, Estruch R, Ros E, Lapetra J, Fito M, Aros F, Serra-Majem L, Lee CH, Clish CB, Liang L, Salas-Salvado J, Martinez-Gonzalez MA, Hu FB. Plasma ceramides, mediterranean diet, and incident cardiovascular disease in the PREDIMED Trial (Prevencion con Dieta Mediterranea). *Circulation* 2017;**135**:2028–2040.
83. Havulinna AS, Sysi-Aho M, Hilvo M, Kauhanen D, Hurme R, Ekroos K, Salomaa V, Laaksonen R. Circulating ceramides predict cardiovascular outcomes in the population-based FINRISK 2002 cohort. *Arterioscler Thromb Vasc Biol* 2016;**36**:2424–2430.
84. Goldenberg JR, Carley AN, Ji R, Zhang X, Fasano M, Schulze PC, Lewandowski ED. Preservation of acyl coenzyme A attenuates pathological and metabolic cardiac remodeling through selective lipid trafficking. *Circulation* 2019;**139**:2765–2777.
85. Li J, Wu W, Xin Y, Zhao M, Liu X. Inhibition of Nogo-B promotes cardiac hypertrophy via endoplasmic reticulum stress. *Biomed Pharmacother* 2018;**104**:193–203.
86. Kong P, Shinde AV, Su Y, Russo I, Chen B, Saxena A, Conway SJ, Graff JM, Frangogiannis NG. Opposing actions of fibroblast and cardiomyocyte smad3 signaling in the infarcted myocardium. *Circulation* 2018;**137**:707–724.
87. Bartke N, Hannun YA. Bioactive sphingolipids: metabolism and function. *J Lipid Res* 2009;**50**(Suppl):S91–S96.
88. Reforgiato MR, Milano G, Fabrias G, Casas J, Gasco P, Paroni R, Samaja M, Ghidoni R, Caretti A, Signorelli P. Inhibition of ceramide de novo synthesis as a postischemic strategy to reduce myocardial reperfusion injury. *Basic Res Cardiol* 2016;**111**:12.
89. Klevstig M, Stahlman M, Lundqvist A, Scharin Tang M, Fogelstrand P, Adiels M, Andersson L, Kolesnick R, Jeppsson A, Boren J, Levin MC. Targeting acid sphingomyelinase reduces cardiac ceramide accumulation in the post-ischemic heart. *J Mol Cell Cardiol* 2016;**93**:69–72.
90. Spassieva SD, Mullen TD, Townsend DM, Obeid LM. Disruption of ceramide synthesis by CerS2 down-regulation leads to autophagy and the unfolded protein response. *Biochem J* 2009;**424**:273–283.
91. Pernet V, Joly S, Dalkara D, Schwarz O, Christ F, Schaffer D, Flannery JG, Schwab ME. Neuronal Nogo-A upregulation does not contribute to ER stress-associated apoptosis but participates in the regenerative response in the axotomized adult retina. *Cell Death Differ* 2012;**19**:1096–1108.
92. Jozsef L, Tashiro K, Kuo A, Park EJ, Skoura A, Albinsson S, Rivera-Molina F, Harrison KD, Iwakiri Y, Toomre D, Sessa WC. Reticulon 4 is necessary for endoplasmic reticulum tubulation, STIM1-Orai1 coupling, and store-operated calcium entry. *J Biol Chem* 2014;**289**:9380–9395.
93. Garcia-Ruiz C, Colell A, Mari M, Morales A, Fernandez-Checa JC. Direct effect of ceramide on the mitochondrial electron transport chain leads to generation of reactive oxygen species. Role of mitochondrial glutathione. *J Biol Chem* 1997;**272**:11369–11377.
94. Quillet-Mary A, Jaffrezou JP, Mansat V, Bordier C, Naval J, Laurent G. Implication of mitochondrial hydrogen peroxide generation in ceramide-induced apoptosis. *J Biol Chem* 1997;**272**:21388–21395.
95. Seddon M, Looi YH, Shah AM. Oxidative stress and redox signalling in cardiac hypertrophy and heart failure. *Heart* 2007;**93**:903–907.
96. Arany Z, Novikov M, Chin S, Ma Y, Rosenzweig A, Spiegelman BM. Transverse aortic constriction leads to accelerated heart failure in mice lacking PPAR-gamma coactivator 1alpha. *Proc Natl Acad Sci U S A* 2006;**103**:10086–10091.
97. Iso T, Haruyama H, Sunaga H, Matsui H, Matsui M, Tanaka R, Umbarawan Y, Syamsunarno M, Putri M, Yamaguchi A, Hanaoka H, Negishi K, Yokoyama T, Kurabayashi M. CD36 is indispensable for nutrient homeostasis and endurance exercise capacity during prolonged fasting. *Physiol Rep* 2018;**6**:e13884.
98. Domarkiene I, Pranculis A, Germanas S, Jakaitiene A, Vitkus D, Dzenkeviciute V, Kucinskiene Z, Kucinskas V. RTN4 and FBXL17 genes are associated with coronary heart disease in genome-wide association analysis of lithuanian families. *Balkan J Med Genet* 2013;**16**:17–22.
99. Jitoku D, Hattori E, Iwayama Y, Yamada K, Toyota T, Kikuchi M, Maekawa M, Nishikawa T, Yoshikawa T. Association study of Nogo-related genes with schizophrenia in a Japanese case-control sample. *Am J Med Genet B Neuropsychiatr Genet* 2011;**156**:581–592.
100. Novak G, Kim D, Seeman P, Tallerico T. Schizophrenia and Nogo: elevated mRNA in cortex, and high prevalence of a homozygous CAA insert. *Brain Res Mol Brain Res* 2002;**107**:183–189.
101. Yang F, Yang S, Liu J, Pang X, Shi F, Qin H, Wang J, Tang R. Impact of RTN4 gene polymorphism and its plasma level on susceptibility to nasopharyngeal carcinoma: a case-control study. *Medicine* 2019; **98**:e17831.
102. Shi S, Zhou B, Wang Y, Chen Y, Zhang K, Wang K, Quan Y, Song Y, Rao L, Zhang L. Genetic variation in RTN4 3'-UTR and susceptibility to cervical squamous cell carcinoma. *DNA Cell Biol* 2012;**31**:1088–1094.